Key Points:
- One lidar model can predict biomass across intact, degraded, and secondary Amazon forests
- Biomass depletion from degradation is large, persistent, and greater from fires than from logging
- Pantropical maps overestimate degraded forest biomass and underestimate intact forest biomass

Aboveground biomass variability across intact and degraded forests in the Brazilian Amazon

Marcos Longo[1], Michael Keller[1,2,3], Maiza N. dos-Santos[1], Veronika Leitold[4], Ekena R. Pinagé[1,5], Alessandro Baccini[6], Sassan Saatchi[3], Euler M. Nogueira[7], Mateus Batistella[8], and Douglas C. Morton[4]

[1]Embrapa Agricultural Informatics, Campinas, Brazil, [2]International Institute of Tropical Forestry, USDA Forest Service, Rio Piedras, Puerto Rico, [3]Jet Propulsion Laboratory, California Institute of Technology, Pasadena, California, USA, [4]NASA Goddard Space Flight Center, Greenbelt, Maryland, USA, [5]Plant Functional Biology and Climate Change Cluster, University of Technology Sydney, Sydney, New South Wales, Australia, [6]Woods Hole Research Center, Falmouth, Massachusetts, USA, [7]National Institute for Research in Amazonia, Manaus, Brazil, [8]Brazilian Agricultural Research Corporation (Embrapa), Brasília, Brazil

Abstract Deforestation rates have declined in the Brazilian Amazon since 2005, yet degradation from logging, fire, and fragmentation has continued in frontier forests. In this study we quantified the aboveground carbon density (ACD) in intact and degraded forests using the largest data set of integrated forest inventory plots ($n = 359$) and airborne lidar data (18,000 ha) assembled to date for the Brazilian Amazon. We developed statistical models relating inventory ACD estimates to lidar metrics that explained 70% of the variance across forest types. Airborne lidar-ACD estimates for intact forests ranged between 5.0 ± 2.5 and 31.9 ± 10.8 kg C m^{-2}. Degradation carbon losses were large and persistent. Sites that burned multiple times within a decade lost up to 15.0 ± 0.7 kg C m^{-2} (94%) of ACD. Forests that burned nearly 15 years ago had between 4.1 ± 0.5 and 6.8 ± 0.3 kg C m^{-2} (22–40%) less ACD than intact forests. Even for low-impact logging disturbances, ACD was between 0.7 ± 0.3 and 4.4 ± 0.4 kg C m^{-2} (4–21%) lower than unlogged forests. Comparing biomass estimates from airborne lidar to existing biomass maps, we found that regional and pantropical products consistently overestimated ACD in degraded forests, underestimated ACD in intact forests, and showed little sensitivity to fires and logging. Fine-scale heterogeneity in ACD across intact and degraded forests highlights the benefits of airborne lidar for carbon mapping. Differences between airborne lidar and regional biomass maps underscore the need to improve and update biomass estimates for dynamic land use frontiers, to better characterize deforestation and degradation carbon emissions for regional carbon budgets and Reduce Emissions from Deforestation and forest Degradation (REDD+).

1. Introduction

Tropical forests are estimated to store between 160 and 250 Pg of carbon (1 Pg = 10^{15} g) or about one fourth of total carbon stocks in land ecosystems [*Sabine et al.*, 2004; *S. Saatchi et al.*, 2011; *Baccini et al.*, 2012]. Carbon stocks in tropical forests are vulnerable to land use changes [*van der Werf et al.*, 2009; *Smith et al.*, 2014; *Le Quéré et al.*, 2015]; however, large uncertainties in tropical forest carbon fluxes arise from difficulties in quantifying forest carbon stocks and carbon stock changes, especially from forest degradation [*Aguiar et al.*, 2012; *Ometto et al.*, 2014; *Bustamante et al.*, 2016]. The goal to Reduce Emissions from Deforestation and forest Degradation (REDD+) is a core component of the Paris Agreement (COP21) [*UN-FCCC*, 2016], and there is an urgent need to quantify the effect of forest degradation on carbon stocks in tropical forests to support REDD+ and improve the accuracy of global carbon budgets [*Bustamante et al.*, 2016; *Morton*, 2016].

The Brazilian Amazon is the largest contiguous area of tropical forest in any country, yet deforestation has already converted nearly 20% of the original extent of forests to pastures or croplands [*Barber et al.*, 2014; *Almeida et al.*, 2016]. Deforestation rates in Brazil have decreased by 70% since 2004 [*Hansen et al.*, 2013; *Nepstad et al.*, 2014]. However, Amazon forest degradation from selective logging, forest fires, and forest fragmentation has continued apace, reducing forest carbon stocks in frontier forests [*Aragão et al.*, 2014; *Berenguer et al.*, 2014; *Pütz et al.*, 2014; *Anderson et al.*, 2015]. Changes in forest structure, species

composition, and successional process from logging and understory fires may last for several decades [*Keller et al.*, 2004a; *Blanc et al.*, 2009; *Alder et al.*, 2012; *West et al.*, 2014; *Rutishauser et al.*, 2016], altering carbon stocks in forests that experience repeated degradation or deforestation [*Morton et al.*, 2013; *Bustamante et al.*, 2016].

Field measurements, experimental studies, and satellite remote sensing provide important insights regarding the magnitude and extent of forest degradation processes in the Amazon. Inventory plots and manipulation experiments to study logging and understory fires are fundamental to understanding the dynamics of degraded forests [e.g., *Blanc et al.*, 2009; *West et al.*, 2014; *Brando et al.*, 2014], but extrapolation from field results is typically limited by the small number of samples, the small area of those samples, and the limited time between repeated samples if there were any repeated samples at all. As a result, the range of degradation impacts on forest structure and carbon stocks across the Amazon remains highly uncertain [*Smith et al.*, 2014; *Bustamante et al.*, 2016]. Satellite-based measurements support degradation mapping over large areas, including remote regions [*Asner et al.*, 2004, 2005; *Morton et al.*, 2013; *Joshi et al.*, 2015], yet the spatial resolution (30–300 m) of satellite imagery most frequently used in land cover change research is insufficient to detect subtle changes in forest structure from low-intensity degradation [*Asner et al.*, 2010]. Cloud cover, a common occurrence in tropical forests, also significantly limits the use of passive optical imagery [*Asner*, 2001].

Airborne lidar provides an intermediate scale between field and satellite-based measurements. Detailed, three-dimensional measurements of forest structure can be obtained using airborne lidar instruments at high resolution (typically 1 m) over thousands of hectares, facilitating forest carbon stock assessments across intact and degraded forest types—even low-intensity disturbances [*Asner et al.*, 2010; *d'Oliveira et al.*, 2012; *Andersen et al.*, 2014]. Airborne lidar data offer the potential to address challenges for REDD+ and tropical forest ecology based on variability in forest carbon stocks at finer spatial scales than satellite observations for current and planned forest carbon mapping efforts [*Morton*, 2016].

Field data, often in combination with satellite data, have been used to generate biomass maps for tropical forests at regional and global scales [e.g., *Saatchi et al.*, 2007; *S. S. Saatchi et al.*, 2011; *Nogueira et al.*, 2008, 2015; *Baccini et al.*, 2012]. Carbon stock estimates are essential to establish REDD+ baselines [*Gibbs et al.*, 2007] and estimate contributions from tropical forest regions to the global carbon budget [*Le Quéré et al.*, 2015]. Although these maps generally agree on average at national or biome scales [*Langner et al.*, 2014], they tend to produce very different estimates at local scales [*Ometto et al.*, 2014]. One fundamental limitation of the first-generation biomass maps based on satellite data is that they are derived from coarse resolution (500–1000 m) remote sensing data with limited sensitivity to fine-scale variations in structure. In addition, few inventory plots in degraded forest types were available for calibration of satellite-based estimates of aboveground biomass. Nevertheless, the disagreement among maps at local scales leads to large uncertainties in carbon emissions, because land cover change from deforestation and forest degradation is concentrated in frontier forest types [*Aguiar et al.*, 2012]. Airborne lidar has the potential to improve regional estimates of biomass by providing detailed information on the regional variability of carbon stocks [*Baccini and Asner*, 2013].

Here we investigated biomass variability in intact and degraded Amazon forest types using the largest integrated inventory plot and airborne lidar data set assembled to date for the Brazilian Amazon. Field samples and coincident lidar acquisitions specifically targeted degraded forest types in order to develop and calibrate a general model of carbon stocks for the Brazilian Amazon that captures different levels of forest degradation and recovery. Lidar-based estimates of aboveground carbon density (ACD) in intact and degraded forests were used to address the following questions:

1. What are the magnitude and duration of ACD differences between intact and degraded forest types?
2. Do differences between airborne lidar and regional and pantropical maps indicate important fine-scale variability in Amazon forest carbon stocks in intact or degraded forest types?

2. Data and Methods
2.1. Study Areas
A total of 18 study areas covering 18,006 ha were selected to evaluate forest carbon stocks in intact and degraded forest types in the Brazilian Amazon (Figure 1), and all data are publicly available at https://www.paisagenslidar.cnptia.embrapa.br/webgis/ and *dos-Santos and Keller* [2016a, 2016b]. Study sites cover a large variation of climate, soils, and land use history, and several sites overlap with focal areas of the Large-Scale
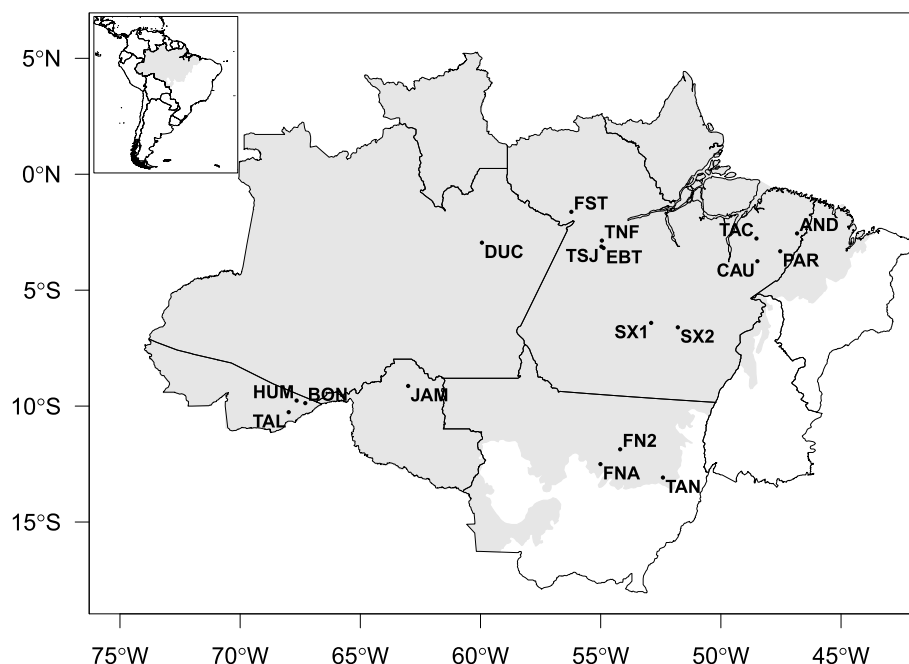
Figure 1. Location of the study areas (dots) in the Brazilian Amazon, where both airborne lidar surveys and forest inventories were obtained. Background corresponds to the Brazilian Amazon Biome (in the sense of *Lapola et al.* [2014]), and contours are Brazilian states. Codes of the study areas are shown next to the respective locations and are defined in Table 1 and Text S1. The exact area of each lidar collection can be visualized in https://www.paisagenslidar.cnptia. embrapa.br/webgis/.

Biosphere-Atmosphere Experiment in Amazonia [*Keller et al.*, 2004b]. All study areas have been surveyed with forest inventories and multiple-return, small-footprint airborne lidar. A brief description of each study area is available online (see Text S1 in the supporting information). We distinguished between sites that experienced recent disturbances such as logging and fire associated with human actions over the last three decades and intact sites for which we have no record or indication of human-induced disturbance.

2.2. Forest Inventories

Forest inventories were conducted at all study sites, and plot measurements included live trees, live palms, woody lianas, and standing dead trees. See Table 1 for a summary of inventory information for all sites. When possible, living individuals were identified from field characteristics by parataxonomists (78% of living individuals), and the decay state of dead individuals was classified following *Harmon et al.* [1995]. A total of 407 forest inventory plots or transect segments (0.25 ha) were included in this study, of which 359 plots were entirely covered by airborne lidar. Remaining plot locations ($n = 48$) were only considered in the analyses of inventory data. Plots and transect segments were classified according to the disturbance history: 128 in intact forests (INT), 76 in reduced-impact logging (RIL), 20 in areas affected by conventional logging (CVL), 17 in areas that burned once (BNO), 32 in areas that were logged and burned once (LBN), and 60 in areas that burned multiple times (BNM). In addition, 20 plots were located in areas of secondary forest (six of them with at least one fire event following regrowth) and 54 in areas that could not be unambiguously classified using Landsat. Plots located in secondary forests or in areas not classified were used for calibration of the airborne lidar model but not included in the analysis by disturbance history.

Most forest inventories used either square plots (40 × 40 m or 50 × 50 m) or fixed-sized transects (20 × 500 m). At Reserva Ducke (DUC), a DBH-dependent probability sampling used 500 m transect lines and included trees that were within a distance of 10 times their DBH on either side of the transect center line [*Hunter et al.*, 2013]. Transects were divided into four separate segments of equal length (five in the case of DUC), similar in area to the square plots. Segment lengths of 100–125 m are much longer than the typical autocorrelation length for aboveground biomass in tropical forests (11 m, following *S. Saatchi et al.* [2011]). Plot size is known to be an important source of errors for calibrating airborne lidar estimates of biomass; while we had a limited range of areas to test the effect of plot size in our calibration, the typical plot area varied between 1600 and 2500 m², a range which has been previously shown to provide stable estimates of tropical forest biomass in Panama

Table 1. Summary of the Data Collected at the Study Areas[a]

Region, State	Site	Site Information			Dry Season	Forest Inventory				Airborne Lidar Survey		
		Longitude	Latitude	Annual Rainfall (mm)	Length (mo)	Date	Count[b]	DBH_0 (cm)	Size (Subsize) (m × m)	Date	Area (ha)	Return Density (m^{-2})
Paragominas region, PA	CAU	48.48 W	3.75 S	2180	5.5	Jan–Mar 2012	85 + 3	10	20(2) × 125	Jul 2012	1214	28.3
	AND	46.83 W	2.55 S	2181	4.9	Aug 2013	20	10	50(5) × 50	Jun 2014	1000	38.2
	PAR	47.53 W	3.32 S	1817	6.0	Mar–Apr 2013	39 + 1	10	20(2) × 125	Jun 2014	1003	40.0
	TAC	48.52 W	2.77 S	2945	3.0	May–Jun 2015	13	5[c]	50(5) × 50	Nov 2013	983	24.2
São Félix do Xingu, PA	SX1	52.90 W	6.41 S	2099	4.1	Oct 2011	9	10	40 × 40	Aug–Sep 2012	993	30.1
	SX2	51.79 W	6.60 S	2157	3.6	Aug 2012	22 + 8	10	40 × 40	Aug–Sep 2012	1005	30.1
Feliz Natal, MT	FNA	55.01 W	12.50 S	1812	5.3	Oct 2013	20	5	50 × 50	Aug 2013	1200	38.3
	FN2	54.19 W	11.86 S	1916	5.4	Aug 2015	7 + 9	10	50(5) × 50	Aug 2013	994	36.5
Fazenda Tanguro, MT	TAN	52.41 W	13.08 S	1767	5.7	Nov 2012	20 + 20	10	20(2) × 125	Aug 2012	1006	13.1
Jamari Natl. Forest, RO	JAM	63.01 W	9.12 S	2054	4.3	Dec 2013	23 + 5	10	50(5) × 50	Sep 2013	1673	31.0
Rio Branco region, AC	BON	67.29 W	9.87 S	2017	4.3	Jul 2014	10	10	50(10) × 50	Sep 2013	600	33.4
	HUM	67.65 W	9.76 S	2012	4.4	Jun–Jul 2014	10	10	50(10) × 50	Sep 2013	501	66.6
	TAL	67.98 W	10.26 S	1980	4.3	Jul 2014	5	10	50(10) × 50	May 2014	500	40.7
Reserva Ducke, AM	DUC	59.94 W	2.95 S	2404	2.8	Sep 2011	25	5	26(★)[d] ×100	Feb 2012	1248	22.7
Saracá-Taquera N.F., PA	FST	56.22 W	1.62 S	2429	4.0	Nov 2013	19 + 1	10	50(5) × 50	Aug 2013	1021	32.9
Belterra region, PA	TNF	54.95 W	2.86 S	2030	4.9	Aug 2013	6	10[e]	50 × 50	Jul/Sep 2012	1049	25.1
	TSJ	54.97 W	3.13 S	2077	5.0	Jul–Aug 2013	12	5–10[e,f]	50 × 50	Sep 2013	1012	30.0
	EBT	54.88 W	3.18 S	2098	4.9	Nov 2014	14 + 1	10	50(5) × 50	Apr 2015	1004	54.9

[a]Brazilian States: Acre (AC), Amazonas (AM), Mato Grosso (MT), Pará (PA), and Rondônia (RO). Annual rainfall and dry season length (number of months with rainfall less than 100 mm) were obtained from the 1998–2015 average of NASA's Tropical Rainfall Measuring Mission and Other Data Precipitation Product 3B43 [Liu et al., 2012]. Forest inventory count is the number of plots or transect segments that overlapped with airborne lidar, and DBH_0 is the minimum diameter at breast height included in the survey. For plots that used subplot, the size for subplot measurements of trees 0–35 cm DBH is given in parentheses.
[b]When shown, counts after the plus sign refer to plots or transects with incomplete lidar coverage, which were only included in inventory analyses (section 3.1) or in the DBH-height allometry (Table S1).
[c]Trees with DBH ≥ 10 cm were measured in the entire plot.
[d]A DBH-dependent sampling was used: trees were measured when their distance from the transect line was less than 10 times their DBH [Hunter et al., 2013]. The transect width corresponds to the largest surveyed individual at DUC (DBH = 128.5 cm).
[e]Living trees, palms, and lianas only.
[f]Five plots used the DBH_0 = 5 cm threshold, while the other seven used DBH_0 = 10 cm.

[*Meyer et al.*, 2013] and in Tanzania [*Mauya et al.*, 2015]. Importantly, plot corners or central transect lines were georegistered with submeter accuracy using differential Global Navigation Satellite Systems (GeoXH6000, Trimble Navigation, Ltd.).

Allometric equations were used to estimate the individual aboveground carbon mass (IAGC, kg C) for trees, palms, and lianas:

1. Living trees, *Chave et al.* [2014]:

$$IAGC = 0.0673 \, f_C \left(\rho_w \, DBH^2 \, H_t \right)^{0.976} , \tag{1}$$

2. Standing dead trees, *Chambers et al.* [2000]:

$$IAGC = 0.1007 \, f_C \, \rho_s \, DBH^2 H_t^{0.818} , \tag{2}$$

3. Living palms, *Goodman et al.* [2013]:

$$IAGC = 0.03781 \, f_C \, DBH^{2.7483} , \tag{3}$$

4. Living lianas, *Schnitzer et al.* [2006]:

$$IAGC = 0.3798 \, f_C \, DBH^{2.657} , \tag{4}$$

where $f_C = 0.5$ is the fraction of oven-dry biomass assumed to be carbon [*Baccini et al.*, 2012], ρ_w and ρ_s are the wood and snag density (g cm^{-3}), DBH is the diameter at breast height (cm), and H_t is the tree height (m). For most sites, H_t was estimated using clinometers; a previous study using inventory data that partially overlap with our data found no statistically significant bias in these height measurements [*Hunter et al.*, 2013]. At five sites where height was not measured for every tree in the field, DBH-height relationships based on Weibull functions [*Feldpausch et al.*, 2012; *Vincent et al.*, 2014] were used to estimate H_t (Table S1).

Wood density was obtained from the *Chave et al.* [2009] and *Zanne et al.* [2009] database. In case multiple values existed for a given species, we took the average of all entries. When only the genus was determined, or when the species was not present at the database, we used the genus average. If both the species and genus were unknown or not available at the database, we used the average wood density for the site. Snag density was assigned using the sample-size weighted average of void-corrected snag density for each decay class at two sites in the Brazilian Amazon [*Palace et al.*, 2007].

2.3. Airborne Lidar Surveys

Airborne lidar surveys were conducted in 2012–2015 using similar data acquisition parameters for all sites. All airborne lidar surveys were carried out by Geoid Laser Mapping Ltda. (Belo Horizonte, Brazil), using lidar instruments with similar characteristics: Surveys in 2012 used an ALTM 3100 (Optech Inc.), data acquired in 2013 and 2014 used ALTM Orion M-200 (Optech Inc.), and flight surveys in 2015 were carried out with an ALTM Orion-M300. Study areas were flown at an average of 850–900 m above ground, and flights had a swath sidelap of 65% and scan angle of 5.5–5.6° off nadir. A minimum return density (≥4 m^{-2} over 99.5% of the study area) was required to avoid inconsistencies and biases in estimated forest properties from low return density [*Jakubowski et al.*, 2013; *Leitold et al.*, 2015]. Average return densities for the study areas were far higher (Table 1).

Lidar data processing followed standard protocols for point cloud analysis and lidar metrics. Data processing was conducted using `FUSION` [*McGaughey*, 2014], and lidar metrics (Table S2) were generated using `R` statistical software [*R Core Team*, 2015]. Lidar metrics were generated for each plot or transect segment to develop lidar-ACD relationships. For spatial analyses and comparisons with regional biomass maps, lidar metrics were computed on regular 50 × 50 m grids at each study site.

2.4. Airborne Lidar Estimates of ACD

To estimate aboveground carbon density based on airborne lidar survey data (ACD$_{ALS}$), we developed a parametric model based on the subset selection of regression method [*Miller*, 1984]. This technique identifies the simplest yet most informative parametric models based on a large number of predictor candidates [e.g., *d'Oliveira et al.*, 2012; *Andersen et al.*, 2014]. To build the model, we carried out the following steps,

using R statistical software: (1) We applied a logarithmic transformation to the field-based ACD and all airborne lidar metrics that were always greater than zero (Table S2) and built a model using all candidate predictors (the full model); only linear terms were included, and we did not consider interaction among predictors. (2) Following *Hudak et al.* [2006], we applied the stepwise subset selection (function stepAIC, package MASS) in the full model, both in forward and in backward modes, to determine the maximum number of parameters that would be allowed. (3) We applied the subset selection of regression in the full model (function regsubsets, package leaps), with exhaustive search and retained only the best subset for each number of parameters, up to the maximum number of parameters allowed (step 2). (4) We back transformed all models selected in step (3) and fitted the coefficients using least squares but allowing for heteroskedastic distribution of residuals [*Mascaro et al.*, 2011a], scaled with the predicted ACD ($E \sim \mathcal{N}\left(\mu = 0, \sigma = \sigma_0 \, \mathrm{ACD}_{\mathrm{ALS}}^q\right)$). (5) For each model fitted in step (4), we calculated the Bayesian Information Criterion (BIC) [*Schwarz*, 1978] and selected the model that produced the lowest BIC statistic.

To assess the model robustness and quantify errors associated with independent predictions of ACD, we applied a cross-validation test based on bootstrap sampling. For each method we applied the following steps: (1) We created a data set replication, in which we selected plots from the full data set using sampling with replacement, with equal probabilities of selecting any plot. For large samples, the bootstrap sampling with equal probabilities includes about 63.2% of unique points from the original data set and the remainder are duplicates [*Efron and Tibshirani*, 1997]. (2) We calibrated the model using the data set replication. (3) The calibrated model was used to predict ACD for the plots that were not included in the data set replication (about 36.8% of the original data set). (4) Steps 1–3 were repeated 1000 times, providing about 368 independent predictions for each plot of the original data set. (5) These independent predictions were compared with the forest inventory estimate of ACD to quantify the goodness of fit.

In addition to the subset selection of regression method, we also tested two nonparametric methods based on regression trees — the Random Forest [*Breiman*, 2001, *Hudak et al.*, 2012; *Mascaro et al.*, 2014] and Generalized Boosted Model [*De'ath*, 2007; *Lloyd et al.*, 2013] and one simpler heteroskedastic model that only depends on the mean top canopy height, which was obtained from the canopy height model. All methods produced fits of similar quality when assessed using cross validation, but the subset selection of regression model had the best agreement with forest inventory estimates of aboveground carbon density and lower BIC than the parametric model using mean top canopy height (Text S2 and Table S3). We therefore present results from the subset selection of regression method; comparisons among methods are included as supporting information (Text S2, Figures S2–S4, S8, and S9, and Table S3).

To evaluate the impact of forest degradation on carbon stocks, we classified the area within each study site according to occurrence of logging and fire. First, we used time series of normalized difference vegetation index (NDVI) and normalized burn ratio (NBR) from Landsat images between 1984 and 2013 to visually identify deforestation, conventional logging, and fire events. For sites with planned, reduced-impact logging operations (CAU, FST, and JAM), the logging companies provided boundaries for annual production units [*MADEFLONA*, 2010; *EBATA*, 2012]. This approach has the advantage of including field knowledge of disturbance histories and longer time series of satellite imagery than available products for detecting and classifying forest degradation [e.g., *Asner et al.*, 2005; *Morton et al.*, 2013; *INPE*, 2014].

Finally, we also developed a model to estimate the total ACD uncertainty for each pixel that accounts for different sources of error, based on *Chave et al.* [2004] and *S. S. Saatchi et al.* [2011]. The main sources of uncertainty were categorized in three components: (1) uncertainty of the forest inventory estimates of ACD used to calibrate the model (calibration uncertainty), (2) the uncertainty due to the limited area surveyed by both the airborne lidar and the ground-based measurements (representativeness uncertainty), and (3) the prediction error due to the ACD variance that cannot be explained by the fitted model (prediction uncertainty). The three error components were aggregated to the pixel level assuming that they were independent and followed normal distributions. Additional details on the error estimates of each component are provided in Text S3. To propagate uncertainties of ACD at coarser resolution and for combined areas of similar disturbance history, we developed a Monte Carlo approach, in which we added a random, normally distributed noise proportional to the uncertainty to each pixel before aggregating the data and used the distribution of 10,000 simulations to obtain the aggregated error.

2.5. Comparison Between Airborne Lidar and Regional Maps of Biomass

We compared three regional maps of carbon stocks to our estimates based on airborne lidar data:

1. *Nogueira et al.* [2015]—N15. A potential biomass map for the Brazilian Amazon, with nominal resolution of 30 m. N15 was developed using a vegetation classification map by *IBGE* [2012]. Biomass values for each land cover class were assigned based on the mean of inventory plots for each land cover class [see also *Nogueira et al.*, 2008].
2. *S. S. Saatchi et al.* [2011]—S11. Pantropical biomass map with resolution of 1 km based on the combination of forest inventory and large-footprint lidar data from the Geoscience Laser Altimeter System (GLAS) on board the Ice, Cloud and land Elevation Satellite (ICESat). The GLAS lidar-biomass model was used to calibrate a wall-to-wall biomass model using reflectance data from Moderate Resolution Imaging Radiometer, a digital terrain model from Shuttle Radar Topography Mission (SRTM), and microwave data from Quick Scatterometer using a maximum entropy model [*Phillips et al.*, 2006].
3. *Baccini et al.* [2012]—B12. A pantropical map with resolution of 463 m that was developed using colocated forest inventory plots and GLAS data. The biomass model obtained from the GLAS data was used to calibrate a wall-to-wall biomass map based on MODIS and SRTM data using a Random Forest model [*Breiman*, 2001].

To ensure that the three regional maps could be directly comparable, we only used the estimates of aboveground biomass carbon density (ABCD) for these maps. For the maps based on airborne lidar, we ran an additional calibration step excluding standing dead trees and generated the maps with 50 m resolution to preserve the definition of airborne lidar metrics selected during the calibration step. In addition, we reprojected all maps to the same grid mesh as B12, which is the coarsest grid that would allow more than one grid point for each study area. Data with finer resolution were aggregated using the R function `rasterize`, with aggregation by averaging.

3. Results

3.1. Variability in Forest Carbon Stocks and Structure From Inventory Data

Aboveground carbon density (ACD) based on forest inventory plots ($n = 407$, from which $n = 359$ were entirely within airborne lidar survey domains) ranged from 0.30 to 39.4 kg C m^{-2}. ACD estimated from forest inventory was typically higher for intact forests and those that were logged using reduced-impact techniques (median values of 17.9 and 17.4 kg C m^{-2}, respectively), whereas plots affected by more intensive or recurrent disturbances such as conventional logging and fires had lower ACD, with median values of 4.8 kg C m^{-2} for areas affected by multiple fires. Inventory plots for moderate degradation classes—conventional logging (CVL) and burned once (BNO)—showed similar median ACD values (7.9–8.6 kg C m^{-2}; Figure 2a), yet similar carbon stock estimates for CVL and BNO arose from different distributions in basal area and wood density (Figures 2b and 2c). The median values of plot-level basal area showed a similar pattern compared to ACD, with higher values observed at plots that were either intact or were disturbed by reduced-impact logging and lowest values at areas affected by multiple fires (Figure 2b). In contrast, the median value for plot-level mean wood density remained similar along the range of forest degradation (0.62–0.73 g cm^{-3}; Figure 2b). The variability of plot-level wood density tended to increase for sites affected by fires: for example, the interquartile range was near 0.06 g cm^{-3} for intact forest plots and 0.17 g cm^{-3} for plots that burned multiple times (Figure 2c).

Degradation type was more important than time since last disturbance for ACD variability in plot data. While both ACD and basal area at disturbed plots were generally lower than at intact forest plots, they did not show a clear tendency following age since last disturbance (Figures 2d and 2e), and this reflects that disturbances of different intensities and recurrences, such as reduced-impact logging and multiple fires, often had similar disturbance age (Figure S6). Plot-level wood density tended to decrease with age since last disturbance, with median values going from 0.75 g cm^{-3}, for plots disturbed less than 2 years, to 0.62 g cm^{-3}, for plots disturbed between 10 and 30 years prior to measurements (Figure 2f), although plots more recently disturbed showed great variability, with interquartile range peaking at 0.13 g cm^{-3} for plots disturbed between 2 and 5 years (Figure 2f). Variability of plot properties was evident even within the same study area, regardless of disturbance history (Figure S6).

Small trees significantly contributed to the total carbon stocks. The median contribution of trees with DBH < 35 cm to total plot ACD ranged between 29 and 61% depending on disturbance history and age since last disturbance, with great variability among plots (Figure S7). The largest variability was observed for plots
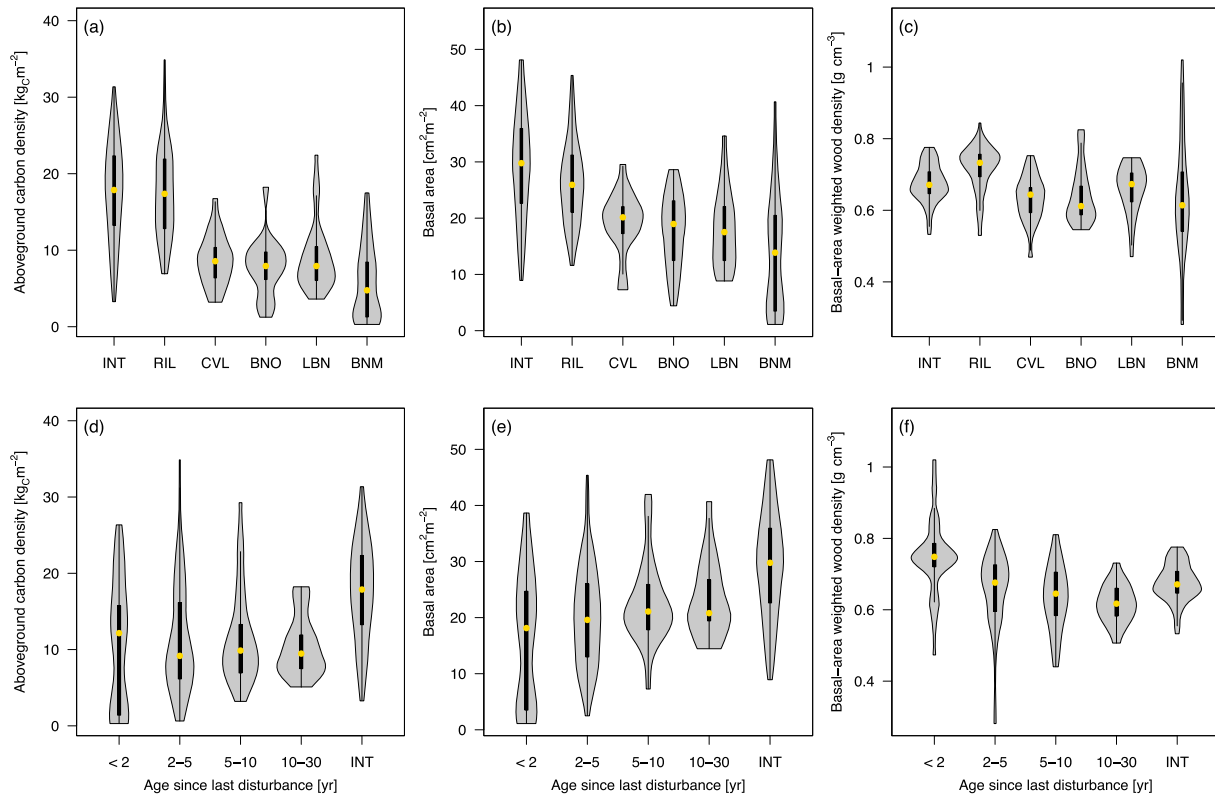
Figure 2. Distribution of plot-level forest characteristics as a function of (a–c) anthropogenic disturbance history and (d–f) age since last disturbance, based on the Landsat chronosequence. Variables shown: aboveground carbon density (ACD) (Figures 2a and 2d), basal area (Figures 2b and 2e), and mean wood density (Figures 2c and 2f), weighted by basal area. The width of the violins is proportional to the kernel density function, black rectangles indicate the interquartile range, and the orange point corresponds to the median. INT—intact; RIL—reduced-impact logging; CVL—conventional logging; BNO—burned once; LBN—logged and burned once; and BNM—burned multiple times. Plots for which disturbance history could not be characterized from Landsat time series and forests with secondary growth were excluded.

affected by recent fires, where the contribution from smaller trees varied from 4 to 100%, suggesting that burned forest shows a broad range of forest structures (Figure S7).

3.2. Calibration of Airborne-Lidar Carbon Density

The best aboveground carbon density model based on airborne-lidar metrics survey (ACD_{ALS}) was

$$ACD_{ALS} = 0.20(0.08)\,\bar{h}^{2.02(0.14)}\,\kappa_h^{0.66(0.13)}\,h_5^{0.11(0.04)}\,h_{10}^{-0.32(0.06)}\,h_{IQ}^{0.50(0.15)}\,h_{100}^{-0.82(0.13)}$$
$$+\,E_{\mathcal{N}}\left[\mu = 0, \sigma = 0.66(0.12)\,ACD_{ALS}^{0.71(0.08)}\right],\tag{5}$$

where $\bar{h}$ is the mean return height, κ_h is the kurtosis of the distribution of all return heights within plot boundaries, h_5 and h_{10} are the 5th and 10th percentiles of all return heights, h_{IQ} is the interquartile range, and h_{100} is the maximum height; $E_{\mathcal{N}}$ is the predicted heteroskedastic distribution of residuals. Numbers in parentheses are the standard errors for each coefficient, obtained from 1000 bootstrap realizations. The variables selected by the subset selection of regression method describe the point cloud distribution at different strata ($h_5, h_{10}, \bar{h}, h_{100}$) and also the general shape of the distribution (h_{IQ}, κ_h), indicating that the structure of the forest beneath the canopy is also relevant for quantifying variability in ACD.

The airborne lidar-ACD relationship was consistent across intact and degraded forest types (Figure 3). Estimates of ACD from airborne lidar and from forest inventory data were strongly correlated ($R^2_{adj} = 0.700$) and with root-mean-square error of 4.17 kg C m^{-2}, comparable to previous studies using field plots of 0.25 ha [e.g., *Asner and Mascaro*, 2014; *Mauya et al.*, 2015; *Réjou-Méchain et al.*, 2015].

Modeled ACD based on lidar data began to saturate above 25 kg C m^{-2} and also tended to slightly overestimate ACD for lower values of ACD_{FI} (Figure S8). On the high end, two phenomena contributed to differences between inventory and lidar-based estimates of ACD. The forest plots that had the highest ACD_{FI} estimates
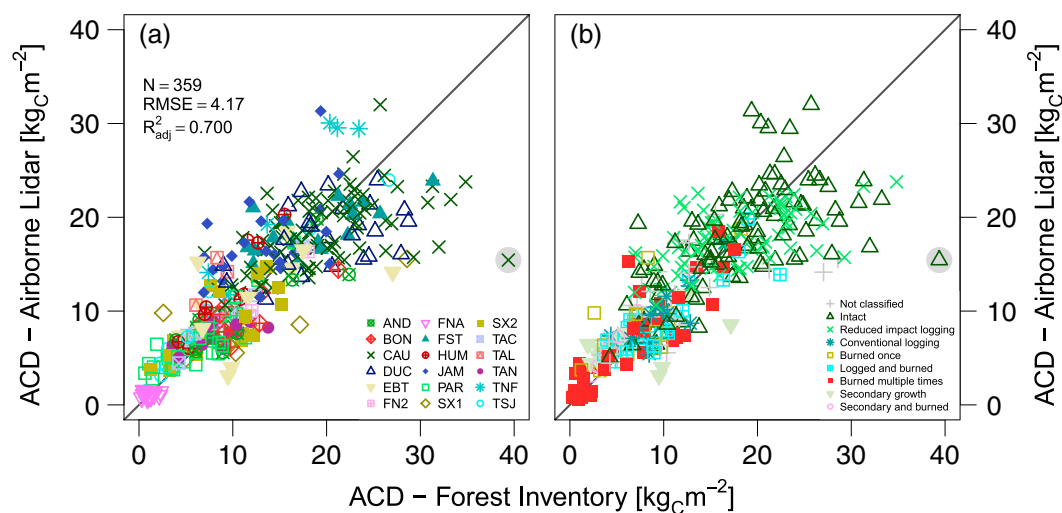
Figure 3. Scatterplots of estimated aboveground carbon density based on airborne lidar metrics using the subset selection of regression (ACD_{ALS}) as a function of forest inventory ACD (ACD_{FI}). Color and shapes correspond to (a) different study sites and (b) different disturbance histories. In both cases the point with the gray shade corresponds to the plot with the largest ACD according to the inventory and the largest absolute residual. The total number of plots, the root-mean-square error (kg C m^{-2}), and the adjusted coefficient of determination are shown in the top left of Figure 3a.

were typically the ones with subsampling and with many trees with DBH just under 35 cm or plots with at least one very large tree (DBH >125 cm). For example, the shaded point in Figure 3 is the plot with the highest residual for all methods and also the highest estimated ACD_{FI} (39.4 kg C m^{-2}). A significant fraction of the total (21.9 kg C m^{-2}) came from a single individual of species *Dinizia excelsa* Ducke, an emergent tree, with DBH = 200.0 cm, H_t = 63.8 m, and ρ_w = 0.905 g cm^{-3}. In contrast, the overestimation of ACD_{ALS} for plots with low ACD_{FI} was mostly associated with plots with low mean wood density (not shown).
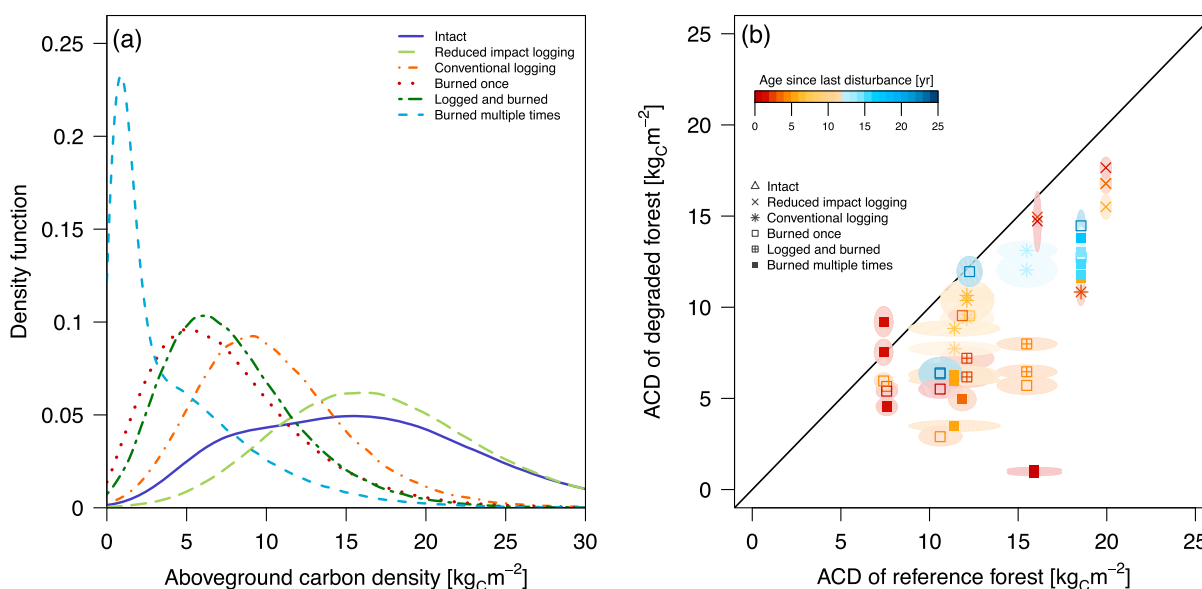

Figure 4. (a) Kernel density estimate of aboveground carbon density (ACD) for all 50 × 50 m pixels from all study areas, separated by disturbance history, excluding those pixels with last disturbance occurring more than 10 years prior to airborne lidar acquisition. Intact forests are areas within the study sites or at nearby sites with no signs of disturbance based on Landsat-derived NDVI and NBR chronosequences between 1984 and 2013. Uncertainty of ACD estimates was incorporated to the curves (see Text S3). (b) Average aboveground carbon density (ACD) of areas that were logged or burned, relative to average ACD of reference (intact) forests. Point shapes correspond to disturbance history, and colors represent the age since last disturbance. Ellipses are the 95% confidence interval of the median value, based on 10,000 replications adding random noise proportional to each pixel uncertainty.

Table 2. Summary of Estimates of Aboveground Carbon Density (ACD, kg C m^{-2}) Based on Airborne Lidar as a Function of Disturbance History[a]

Site	History	Area	ACD_{25}	ACD_{50}	$\overline{ACD}$	ACD_{75}	ΔACD_{50}	$\Delta \overline{ACD}$
CAU	INT	594.75	15.34 ± 0.16	19.81 ± 0.21	20.45 ± 0.16	24.97 ± 0.19	—	—
	RIL (2006)	100.00	11.33 ± 0.34	15.33 ± 0.43	16.21 ± 0.33	20.35 ± 0.44	−4.48 ± 0.47	−4.24 ± 0.36
	RIL (2007)	160.75	12.57 ± 0.28	16.63 ± 0.35	17.30 ± 0.27	21.42 ± 0.34	−3.18 ± 0.41	−3.16 ± 0.32
	RIL (2008)	192.25	12.51 ± 0.25	16.64 ± 0.33	17.44 ± 0.25	21.67 ± 0.32	−3.17 ± 0.39	−3.01 ± 0.30
	RIL (2010)	155.25	13.39 ± 0.29	17.54 ± 0.37	18.30 ± 0.29	22.45 ± 0.36	−2.27 ± 0.43	−2.15 ± 0.33
AND	INT	23.00	11.81 ± 0.68	15.49 ± 0.87	15.97 ± 0.66	19.73 ± 0.80	—	—
	BRN (2009)	72.75	2.73 ± 0.16	5.71 ± 0.26	6.76 ± 0.19	8.64 ± 0.31	−9.78 ± 0.91	−9.20 ± 0.69
	CVL (1999) and BRN (2009)	213.50	5.40 ± 0.14	7.99 ± 0.18	8.83 ± 0.14	11.48 ± 0.20	−7.50 ± 0.89	−7.14 ± 0.68
	CVL (2003) and BRN (2009)	130.50	4.35 ± 0.15	6.46 ± 0.19	7.11 ± 0.15	9.22 ± 0.21	−9.03 ± 0.89	−8.85 ± 0.68
PAR	INT	3.50	8.71 ± 1.35	11.41 ± 1.33	11.46 ± 1.04	14.13 ± 1.45	—	—
	CVL (1993) and CVL (2006)	99.25	6.40 ± 0.22	8.84 ± 0.22	9.12 ± 0.16	11.55 ± 0.26	−2.57 ± 1.35	−2.34 ± 1.05
	BRN (2005) and BRN (2008)	48.50	4.15 ± 0.25	6.28 ± 0.26	6.70 ± 0.19	8.79 ± 0.33	−5.13 ± 1.35	−4.76 ± 1.06
	CVL (1993) and BRN (1992, 2005, 2008)	52.50	2.23 ± 0.15	3.49 ± 0.15	3.77 ± 0.12	4.98 ± 0.20	−7.91 ± 1.34	−7.70 ± 1.05
	CVL (1993, 2006) and BRN (1992, 2008)	176.50	4.07 ± 0.12	5.98 ± 0.13	6.36 ± 0.10	8.23 ± 0.16	−5.43 ± 1.34	−5.11 ± 1.05
SX1	INT	15.25	7.83 ± 0.63	10.60 ± 0.62	10.90 ± 0.47	13.63 ± 0.74	—	—
	BRN (2007)	16.00	1.61 ± 0.22	2.90 ± 0.28	3.57 ± 0.21	4.84 ± 0.42	−7.70 ± 0.68	−7.33 ± 0.52
	BRN (2011)	44.75	3.46 ± 0.22	5.51 ± 0.26	6.63 ± 0.20	8.46 ± 0.39	−5.08 ± 0.67	−4.27 ± 0.51
SX2	INT	40.00	5.36 ± 0.31	7.58 ± 0.31	7.98 ± 0.23	10.15 ± 0.38	—	—
	BRN (2008)	174.25	3.58 ± 0.12	5.66 ± 0.13	6.12 ± 0.09	8.13 ± 0.17	−1.93 ± 0.33	−1.86 ± 0.25
	BRN (2010)	56.00	3.40 ± 0.20	5.40 ± 0.22	5.86 ± 0.16	7.80 ± 0.29	−2.18 ± 0.38	−2.12 ± 0.29
	BRN (2008, 2010)	146.75	2.82 ± 0.11	4.61 ± 0.12	5.16 ± 0.09	6.91 ± 0.17	−2.98 ± 0.33	−2.83 ± 0.25
	BRN (1990, 2008, 2010)	33.00	2.90 ± 0.23	4.55 ± 0.25	4.99 ± 0.19	6.64 ± 0.34	−3.03 ± 0.39	−2.99 ± 0.30
FNA	INT	18.25	12.04 ± 0.79	15.90 ± 0.78	16.32 ± 0.58	20.18 ± 0.93	—	—
	BRN (2005, 2007, 2010, 2012)	36.25	0.53 ± 0.07	1.04 ± 0.08	1.16 ± 0.06	1.62 ± 0.10	−14.86 ± 0.79	−15.1 ± 0.58
	CVL (1992) and BRN (2005, 2007, 2010, 2012)	49.00	0.57 ± 0.07	1.08 ± 0.07	1.27 ± 0.06	1.72 ± 0.09	−14.82 ± 0.79	−15.0 ± 0.58
	CVL (1997) and BRN (2005, 2007, 2010, 2012)	206.50	0.45 ± 0.03	0.93 ± 0.03	1.06 ± 0.02	1.50 ± 0.04	−14.97 ± 0.78	−15.2 ± 0.58
	CVL (1999) and BRN (2005, 2007, 2010, 2012)	304.00	0.53 ± 0.03	1.04 ± 0.03	1.17 ± 0.02	1.64 ± 0.03	−14.86 ± 0.78	−15.1 ± 0.58
TAN	INT	698.75	5.31 ± 0.07	7.41 ± 0.07	7.64 ± 0.05	9.72 ± 0.08	—	—
	CTL	50.00	5.32 ± 0.27	7.41 ± 0.27	7.60 ± 0.21	9.67 ± 0.31	—	—
	BRN (2007)	50.00	4.20 ± 0.23	5.95 ± 0.23	6.14 ± 0.17	7.88 ± 0.26	−1.46 ± 0.35[b]	−1.46 ± 0.27[b]
	BRN (2004, 2007, 2010)	50.00	3.63 ± 0.32	7.54 ± 0.37	8.16 ± 0.24	11.70 ± 0.49	+0.13 ± 0.46[b]	+0.56 ± 0.32[b]
	BRN (2004–2007, 2009–2010)	50.00	5.34 ± 0.35	9.21 ± 0.42	10.28 ± 0.29	14.32 ± 0.60	+1.79 ± 0.50[b]	+2.69 ± 0.36[b]
JAM	INT	1001.50	12.18 ± 0.11	16.09 ± 0.11	16.59 ± 0.08	20.43 ± 0.13	—	—
	RIL (2010)	100.00	11.22 ± 0.32	14.95 ± 0.32	15.37 ± 0.24	19.02 ± 0.38	−1.14 ± 0.34	−1.23 ± 0.25
	RIL (2012)	13.25	11.28 ± 0.86	14.70 ± 0.85	15.13 ± 0.65	18.58 ± 1.02	−1.38 ± 0.86	−1.47 ± 0.65
	RIL (2013)	411.50	11.56 ± 0.16	15.41 ± 0.16	16.05 ± 0.12	19.83 ± 0.20	−0.67 ± 0.19	−0.54 ± 0.15
BON	INT	18.50	9.15 ± 0.62	12.10 ± 0.76	12.57 ± 0.61	15.47 ± 0.72	—	—
	CVL (2006)	247.25	7.77 ± 0.16	10.65 ± 0.20	11.21 ± 0.15	14.11 ± 0.20	−1.45 ± 0.79	−1.36 ± 0.63
	BRN (2010)	23.00	3.87 ± 0.34	6.39 ± 0.46	7.03 ± 0.35	9.04 ± 0.51	−5.71 ± 0.89	−5.54 ± 0.70
	CVL (2002) and BRN (2010)	51.75	4.93 ± 0.26	7.20 ± 0.32	7.97 ± 0.26	10.23 ± 0.37	−4.90 ± 0.83	−4.60 ± 0.66
	CVL (2006) and BRN (2010)	52.00	4.00 ± 0.23	6.17 ± 0.29	7.02 ± 0.23	9.10 ± 0.36	−5.92 ± 0.81	−5.55 ± 0.65
HUM	INT	62.25	8.92 ± 0.35	12.25 ± 0.36	12.90 ± 0.27	16.16 ± 0.46	—	—
	BRN (2005)	78.50	6.53 ± 0.27	9.53 ± 0.28	10.15 ± 0.20	13.11 ± 0.36	−2.72 ± 0.45	−2.75 ± 0.34

Table 2. (continued)

Site	History	Area	ACD_{25}	ACD_{50}	$\overline{ACD}$	ACD_{75}	ΔACD_{50}	$\Delta\overline{ACD}$
TAL	INT	46.75	8.73 ± 0.39	11.86 ± 0.39	12.41 ± 0.30	15.48 ± 0.49	—	—
	BRN (2010)	201.75	6.56 ± 0.17	9.54 ± 0.17	10.12 ± 0.12	13.02 ± 0.22	-2.32 ± 0.43	-2.30 ± 0.32
	BRN (2005, 2010)	22.25	3.22 ± 0.29	4.96 ± 0.32	5.60 ± 0.25	7.38 ± 0.46	-6.90 ± 0.51	-6.81 ± 0.39
FST	INT	207.25	14.00 ± 0.26	18.45 ± 0.26	19.01 ± 0.19	23.41 ± 0.32	—	—
	RIL (2013)	796.00	13.62 ± 0.13	17.77 ± 0.13	18.29 ± 0.10	22.35 ± 0.15	-0.69 ± 0.29	-0.73 ± 0.21
EBT	INT[c]	1048.75	13.46 ± 0.12	18.55 ± 0.13	19.31 ± 0.09	24.30 ± 0.15	—	—
	BRN (1997, 2004)	34.25	11.04 ± 0.53	14.39 ± 0.51	14.65 ± 0.39	17.97 ± 0.59	-4.15 ± 0.53	-4.66 ± 0.40
	BRN (1992, 1997, 2009)	63.75	8.35 ± 0.34	11.60 ± 0.34	12.00 ± 0.25	15.21 ± 0.42	-6.95 ± 0.36	-7.31 ± 0.27
	CVL (2012)	51.75	7.63 ± 0.35	10.83 ± 0.37	11.65 ± 0.27	14.79 ± 0.49	-7.71 ± 0.39	-7.65 ± 0.29

[a]History classes: INT—intact; CTL—control (fire experiment); BRN—burned; CVL—conventional logging; and RIL—reduced-impact logging. Area—total area in ha; ACD_{25}—lower quartile, ACD_{50}—median, $\overline{ACD}$—mean, and ACD_{75}—upper quartile; ΔACD_{50} and $\Delta\overline{ACD}$—the absolute difference in median and mean value between degraded and intact. Standard error was obtained from 10,000 replications, in which we applied random noise proportional to each pixel uncertainty and aggregated values for each area. We show up to four largest disturbance classes for each study area (excluding secondary forests) and restricted to areas where the last disturbance occurred within 10 years prior to the airborne lidar acquisition.
[b]Relative to control.
[c]Intact area is at the TNF site, 18–48 km northwest of the EBT areas.

The residual dependence on ACD was not associated with geographic location, data acquisition characteristics, terrain complexity, or forest structure. First, the residuals of ACD_{ALS} did not show significant differences between intact, degraded, and secondary forests (Figures 3b and S9), and, except for a smaller spread for the most degraded sites, residuals did not show any pattern that could be linked to individual site characteristics (Figure S10a). Residuals were also not correlated to mean top canopy height, also indicating that the method is not consistently biased for intact forests or very degraded areas (Figure S10b). Likewise, the residuals do not show any dependence on return density (Figure S10c) or local terrain roughness (Figure S10d), and in both cases the largest spread of residuals was found near the median values instead of the extremes.

3.3. Impact of Forest Degradation on Carbon Stocks
Carbon stocks in intact forests showed large variability within and across study sites. The main peak of the aggregated distribution was near 15.6 kg C m^{-2}, based on the concentration of intact forests in central Amazon sites (DUC, TNF, FST, CAU, and JAM). The distribution of ACD for intact forests is nearly flat topped: density estimates were similar to peak for ACD values as low as 7.0 kg C m^{-2}, because of the ACD contribution of intact but transitional forests at TAN and SX2 (Figure 4a and Table 2). The range of carbon density of intact forests was broad, and 95% of the intact forests had values between 4.9 and 29.8 kg C m^{-2}. The local interquartile range of ACD for intact forests for all study areas was typically of the order of 45–60% of the median value for each study area, indicating important natural variability of carbon stocks both within and across sites (Table 2).

Carbon stocks in logged forests were generally lower than in intact forests, and the magnitude of differences depended on forest management and time since logging. Areas that were logged using reduced-impact techniques had a peak in the distribution similar to the one for intact forests, being 0.2 kg C m^{-2} (1.5%) higher than the main peak for intact forests (Figure 4a), because reduced-impact logging occurred at study areas with high reference ACD (CAU, FST, and JAM, Table 2), Nonetheless, the median ACD was small but still significantly lower by 0.7 ± 0.3 to 4.4 ± 0.4 kg C m^{-2} (4–22%) relative to nearby intact areas (Figure 4b and Table 2). The peak associated with conventional logging without fires was about 9.0 kg C m^{-2} (42.3%) lower than in intact forests (Figure 4a), and the median depletion at the site level varied from 1.5 ± 0.8 to 7.7 ± 0.4 kg C m^{-2} (12–42%), with highest depletion at the most recently logged site (EBT, Figure 4b and Table 2).

Burned forests had significantly lower carbon stocks. The peak of the distribution of areas that burned once was between 9.3 and 10.0 kg C m^{-2} (60–65%) lower than the main peak for intact forests (Figure 4a). Areas subject to multiple fires had the lowest carbon stocks, and the peak of the distribution occurred at 0.9 kg C m^{-2} or 94% less than the main peak for intact forests. While the depletion of carbon stocks associated with burned forests was typically large, the difference between burned areas and nearby reference areas was extremely variable, even in the case of multiple fires. For example, the areas subject to three experimental fires in TAN
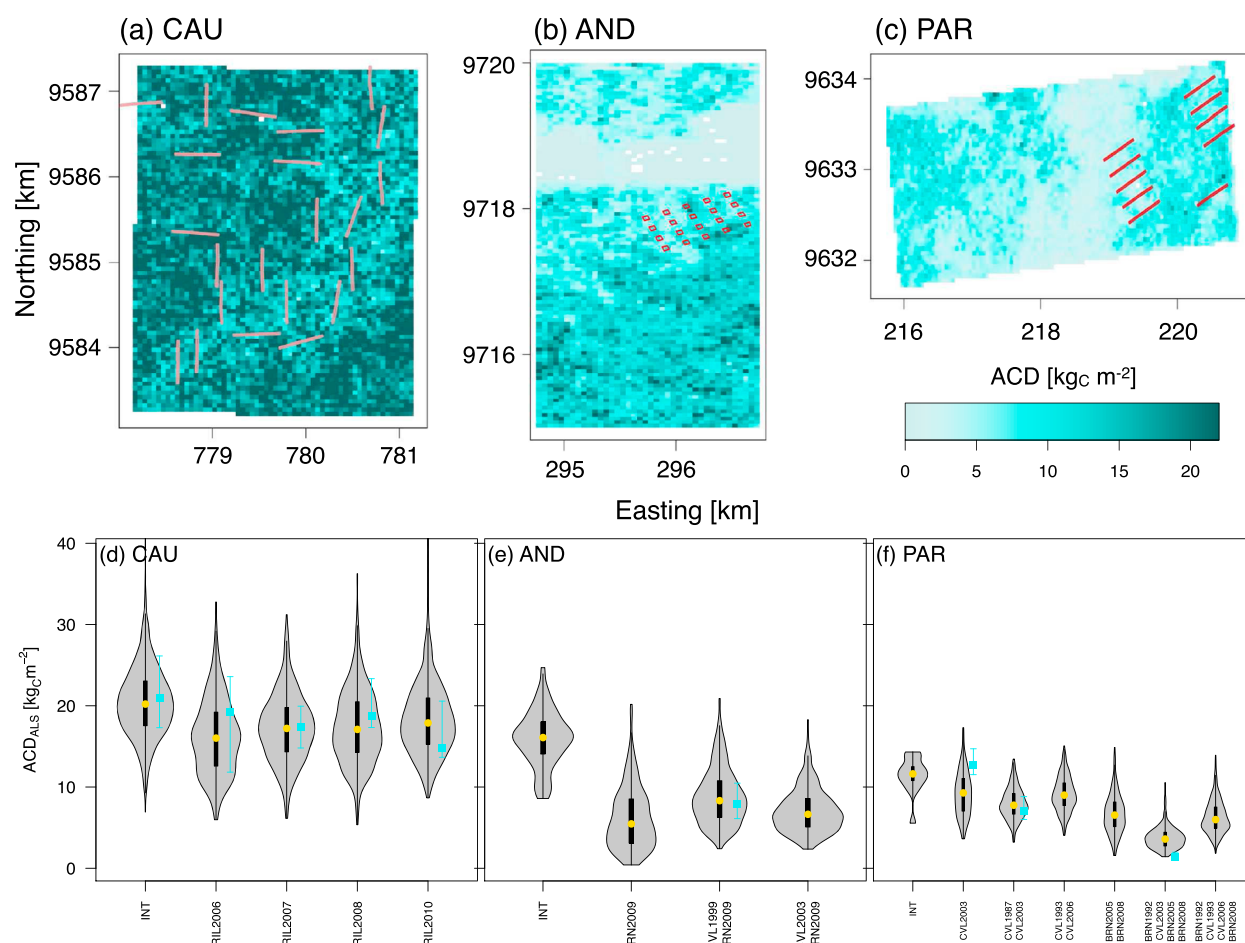
Figure 5. Aboveground carbon density predicted by airborne lidar (ACD_{ALS}, 50×50 m grid) for the three study areas in the Paragominas municipality. Wall-to-wall maps for (a) Fazenda Cauaxi (CAU), (b) Fazenda Andiroba (AND), and (c) Fazenda Nova Neonita (PAR); lines show the location of forest inventory transects (Figures 5a and 5c) and plots (Figure 5b). Violin plots of ACD separated by disturbance history at (d) CAU, (e) AND, and (f) PAR. The width of the violins is proportional to the kernel density function, black rectangle corresponds to the interquartile range, the orange point corresponds to the median estimated by airborne lidar, the blue box corresponds to the median ACD_{FI}, and lines correspond to the interquartile range for individual plots. INT — intact; RIL — reduced-impact logging (and year); CVL — conventional logging (and year); and BRN — burned (and year).

showed no significant difference in median and mean ACD (Table 2), whereas the area that was burned six times showed higher median ACD (1.8 ± 0.5 kg C m^{-2}) than the control (intact) area, although these results may indicate a limitation of our method to detect low-intensity disturbances. TAN experimental fires were low intensity and caused higher mortality among smaller trees [*Brando et al.*, 2014], which likely left the forest with high canopy cover and thinner understory in a way not captured by any of the calibration plots. At the experimental sites, the top canopy height (TCH) model was closer to expectation from published ground-based estimates (Figure S11) [*Brando et al.*, 2014]. On the other hand, the TCH model shows significant differences between the control area and the remaining areas of intact forest, whereas the ALS model shows closer agreement as expected. For other sites, the areas affected by four intense fires between 2005 and 2012 in FNA showed median ACD depletions of up to 15.0 ± 0.8 kg C m^{-2} (94%, Table 2), and the large sampled area affected by these fires contributed to the strong peak in distribution at low values (Figure 4a). The effects of forest fires were persistent: the median ACD for areas that burned during the 1991/1992 and 1997/1998 droughts at TSJ and EBT were 4.1 ± 0.5 to 7.7 ± 0.4 kg C m^{-2} (22–42%) lower than at nearby intact forests at TNF (age of last disturbance of 16–18 years: Figure 4b).

In general, forest inventories were not designed to represent biomass variability at individual sites, and therefore, they characterize only part of the variability of carbon stocks across intact and degraded forests captured by airborne lidar surveys. Figure 5 illustrates differences between plot and lidar estimates for three study areas in Paragominas (CAU, AND, and PAR) with different forest degradation histories. At CAU, forest transects were
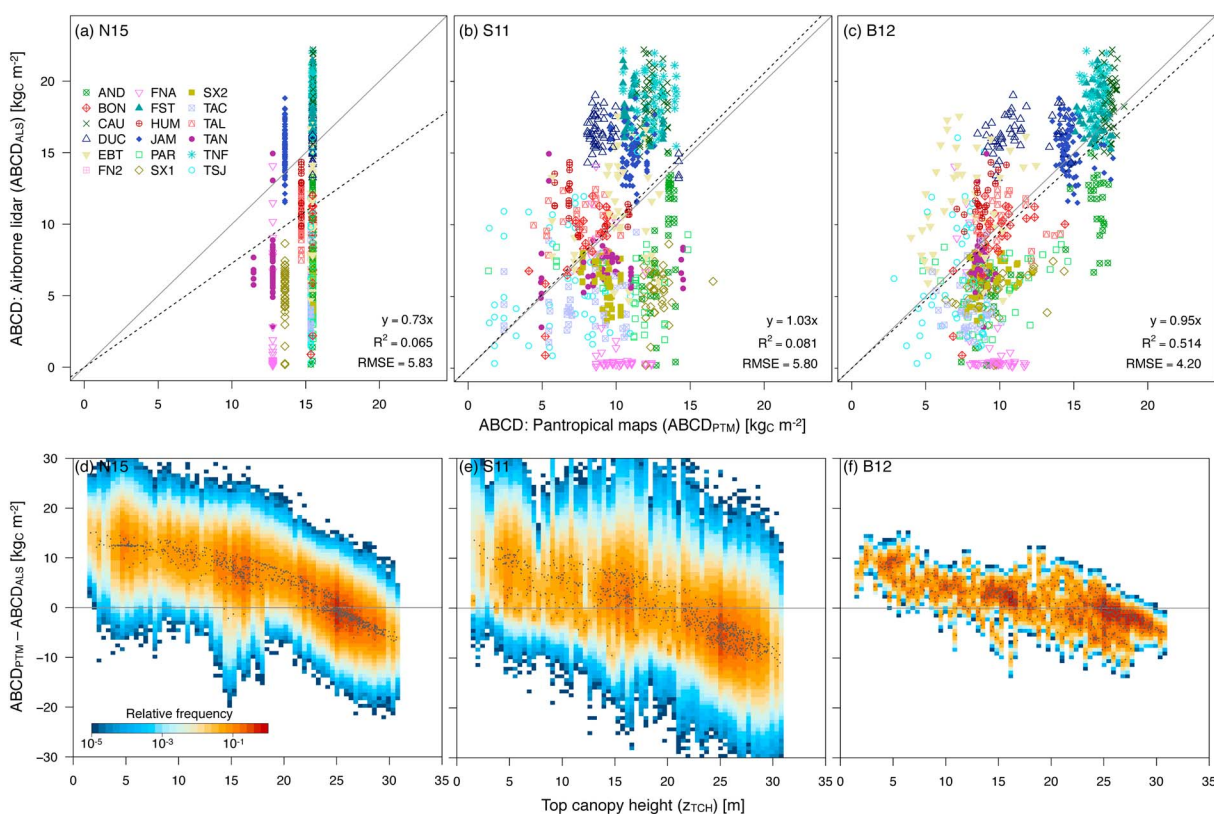
Figure 6. Scatterplot of aboveground carbon density based on pantropical maps (ABCD$_{PTM}$) of (a) *Nogueira et al.* [2015] (N15), (b) *S. S. Saatchi et al.* [2011] (S11), and (c) *Baccini et al.* [2012] (B12) against the ABCD estimated by the airborne lidar metrics (ABCD$_{ALS}$). The solid line is the 1:1 line, and the dashed line represents the slope of the $y = a x$ curve fitted with ordinary least squares, summarized at the bottom right of each panel. Scatterplot of the mean top-of-canopy height and the difference in ABCD between pantropical maps and the airborne lidar model (ABCD$_{PTM}$ − ABCD$_{ALS}$): (d) *Nogueira et al.* [2015] (N15), (e) *S. S. Saatchi et al.* [2011] (S11), and (f) *Baccini et al.* [2012] (B12). The heat maps in the background of Figures 6d–6f indicate the relative frequency generated by 10,000 realizations in which random noise was added to each pixel, proportional to uncertainties in ABCD$_{PTM}$ and ABCD$_{ALS}$.

distributed across most of the study area (Figure 5a) and forest inventories characterized the median value of all disturbance classes within the interquartile range of estimated ACD based on airborne lidar (Figure 5d). At AND, plots sampled forest that were logged in 1999 and burned in 2009 and characterized the variability in this disturbance class (Figure 5e), but they could not represent the median or variability of intact forests and areas that were logged and burned, even though both classes had significant extent in the study area. Similarly, the transects at PAR were concentrated in the eastern portion of the airborne lidar survey, forests that were logged in 2003 and either never burned or burned three times (1992, 2005, and 2008). Regions that were only logged in 2003 occur in the southeastern part of the study site, and only three transect segments overlapped with the region of higher predicted ACD (Figures 5c and 5f). The northeastern portion of the study site was logged twice (1987 and 2003), and 12 transect segments were within this region, resulting in closer distribution between airborne lidar and field inventory plot distribution of ACD (Figures 5c and 5f). Only three transect segments were within the area logged in 2003 and burned three times, and the airborne lidar only characterized the lowest values (Figures 5c and 5f), whereas the region deforested in 1990 followed by secondary growth along the central region did not have any transects, which were concentrated at the higher ACD region near the edge of the deforested area (not shown).

3.4. Comparison With Pan-Amazonian Maps of Biomass

The comparison between airborne lidar estimates of aboveground biomass carbon density (ABCD$_{ALS}$; see Text S4 for model) and the pan-Amazonian maps of biomass showed generally low agreement and large discrepancies in range. The *Nogueira et al.* [2015] estimate (N15) had a narrow range of ACD compared to ABCD$_{ALS}$, resulting in a low slope and low coefficient of determination for the linear fit between the N15 and ALS maps (Figure 6a). Although the map by *S. S. Saatchi et al.* [2011] (S11) has a broader range of values compared to N15 and the slope is closer to one, the correlation between the S11 and the airborne lidar estimates was also
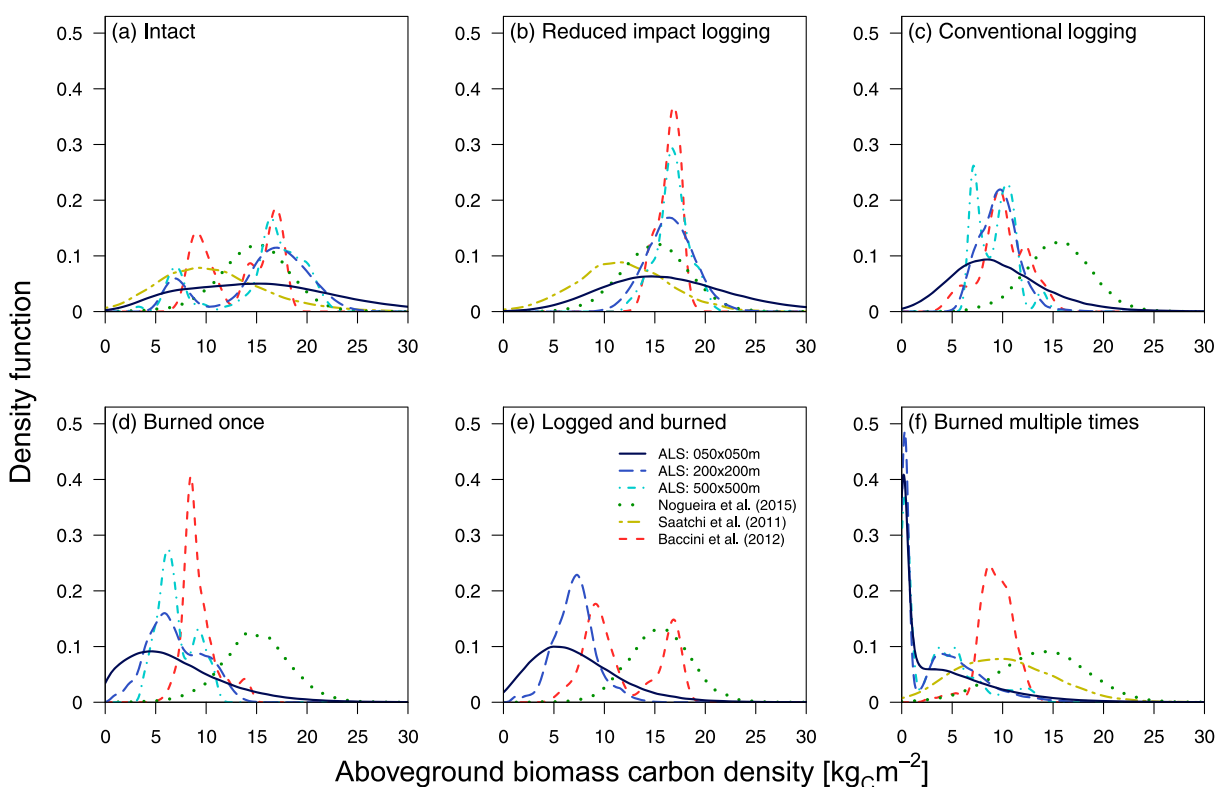
Figure 7. Density function of aboveground biomass carbon density (ABCD) for all study sites combined as a function of disturbance history. The following ABCD estimates are included: airborne lidar estimate (ALS) at native resolution (50 m), and aggregated at 200 m and 500 m, from *S. S. Saatchi et al.* [2011], *Baccini et al.* [2012], and *Nogueira et al.* [2015] maps. The disturbance history categories were derived from the Landsat chronosequence and from the logging company reports when available: (a) Intact, (b) reduced-impact logging, (c) conventional logging, (d) one fire occurrence, (e) logging and one fire event, and (f) multiple fires. For each class, we only estimated density functions for maps with at least 20 pixels. Uncertainty in pixel estimates of ACD were propagated to density curves following method described in Text S3.

low ($R^2 = 0.08$, Figure 6b). The best agreement between airborne lidar and pan-Amazonian maps was found for the *Baccini et al.* [2012] (B12) map, where the slope between the maps is close to one, and the coefficient of determination was above 0.5 (Figure 6c). The higher R^2 in the B12 case results from B12 showing greater ABCD variability among sites, although the local variability of ABCD is generally small compared to the airborne lidar method (Figure 6c). In addition, all maps rarely showed low biomass values at the study sites relative to the airborne lidar estimate: using ABCD = 5 kg C m^{-2} as reference for low biomass, we found that 19.6% of the pixels were below the reference according to the airborne lidar, whereas only 1.3% and 3.9% of the pixels were considered low biomass according to B12 and S11, respectively. None of the N15 pixels were below this category, and the pixel with the lowest biomass among the study areas according to N15 had a potential ABCD of 11.5 kg C m^{-2}.

Carbon stocks for intact forests from regional maps tended to be lower than carbon stocks from the airborne lidar model. At regions with mean top canopy height higher than 25 m, estimates of ABCD from all regional maps are lower than the airborne lidar estimate, in particular for the S11 map (Figures 6d–6f); similarly, the aggregated distribution of ABCD for regions classified as intact for the S11 map has a peak that is 6.0–7.7 kg C m^{-2} lower than the main peak for airborne lidar estimates (Figure 7a). In contrast, the shape of the distribution for B12 at intact forest was closer to the distribution predicted by airborne lidar, particularly when the airborne lidar estimates are aggregated to 500 m (Figure 7a).

Carbon stocks from all three regional maps were higher than airborne lidar estimates for degraded forests, in particular for burned areas. In areas with low mean top canopy height (z_{TCH}), typical of degraded forests, values of ABCD from regional maps were 7–15 kg C m^{-2} higher than airborne lidar estimates (Figures 6d–6f), with the largest differences occurring for comparison between airborne lidar and N15 for the lowest z_{TCH} (Figure 6d). The differences between regional maps and airborne lidar were also dependent upon the

disturbance level. For areas with light disturbance such as reduced-impact logging, the distribution peak of airborne lidar is similar to N15, and the distribution of airborne lidar estimates compared well with B12, especially when lidar was aggregated to 500 m (Figure 7b). Burned forests showed far higher ABCD from the regional maps than from the airborne lidar model, with the B12 distribution shifted 3.9 kg C m^{-2} (85%) higher than the airborne lidar distribution and the N15 map 9.8 kg C m^{-2} (208%) higher than the airborne lidar estimates (Figure 7d). Differences in carbon density between regional maps and airborne lidar model were even more extreme for regions that burned multiple times, where the distribution peaks of the B12 and N15 maps were 8.5 kg C m^{-2} and 13.7 kg C m^{-2} higher than the predicted peaks estimated by airborne lidar. A similar analysis of the density functions was also conducted using the MODIS Vegetation Continuous Fields product (MOD44B) [*Hansen et al.*, 2005; *Townshend et al.*, 2001] to classify the forests by degradation level using an independent data set, and results also show greater agreement between lidar and N15, S11, and B12 at areas with high fractional tree cover and decrease in estimated ABCD estimates by lidar at regions with lower tree cover, while the regional maps show less variation between the different classes of tree and vegetation cover fraction (Figure S12).

4. Discussion

In this study we used the most extensive data set of integrated forest inventory plots and airborne lidar surveys assembled for the Brazilian Amazon to characterize biomass variability in intact and degraded forests. Degraded forests were well characterized by the combination of inventory plots and airborne lidar data, but the large range of degradation impacts was not fully captured by inventory plots (sample area of 0.25 ha) or regional biomass maps (pixel area of 25–100 ha) Differences between degraded and intact forest ACD were the greatest for burned forests, yet degraded forests showed persistent differences over the range of time since last disturbance — up to 23 years at our study sites. Plot size also influenced our model results. Smaller plots (0.25 ha in this study) may increase the variability in plot ACD, based on the influence of large trees and plot edge effects [*Mascaro et al.*, 2011b; *Mauya et al.*, 2015]. Biomass variability found in this study has important implications for Amazon forest carbon monitoring and emissions estimates for REDD+. Our study provided ACD estimates for 7000 ha of degraded forests. Patterns that emerge from our work suggest that fires have greater impact on ACD losses than logging, ACD losses are persistent, and ACD in dynamic forest frontiers shows important differences with first-generation biomass maps in both intact (airborne lidar is 3–34% higher than the pan-Amazonian maps) and degraded (airborne lidar is 2–67% lower than the pan-Amazonian maps) forests (Table S4), with important impacts on REDD+ accounting and estimates of forest carbon emissions in the global carbon budget.

4.1. Simple, Parametric Methods Are Robust to Estimate Carbon Stocks

Forest inventory plots used as reference for the model calibration covered a broad range of landscapes and provided critical information on the variability of forest properties across intact and degraded forests. In particular, the data set showed that the lower carbon stocks at the most degraded forests arose from a combination of lower basal area and higher frequency of plots dominated by low wood density trees (Figure 2). These results highlight that lower carbon stocks in degraded forests emerged from changes in structure and composition. Larger trees have a significant role on the variability in carbon stocks [*Slik et al.*, 2013], as a single large tree could contribute to more than half of the total estimated carbon stocks (Figure 3). However, we also found that small trees significantly contributed to the total carbon stocks. The typical contribution of trees with DBH < 35 cm to total ACD was between 17 and 46%. For many sites included in this study, small trees were measured in subplots of 10–20% of the total area; we could have reduced uncertainty by increasing the subsample area or measuring trees with DBH above 10 cm for the entire plot, although this would increase or field survey costs substantially as the costs scaled more closely with the number of trees surveyed as opposed to the area surveyed. Also, the size of field plots used in the calibration step (0.25 ha) were relatively small for calibrating airborne lidar in tropical forests. Smaller plots yield to large variability in field plot estimates of ACD due to the presence or absence of large trees in the plot and also to representativeness issues due to a large fraction of the plot containing canopy trees that are partially inside or partially outside the domain [*Mascaro et al.*, 2011b]. Future studies at a regional scale might benefit from the use of larger plots (1 ha) for model calibration [*Mauya et al.*, 2015; *Réjou-Méchain et al.*, 2015; *Molina et al.*, 2016], yet even larger plots may not capture patterns of biomass variability in degraded forests (see Figure 5).

A simple parametric model captured a significant fraction of carbon density variability across intact and degraded forests in the Brazilian Amazon. The selected model combined airborne lidar metrics that described

the vertical structure of the forest, with specific sensitivity to canopy openness and canopy roughness captured by lower height profiles and higher moments of the lidar return distribution. The airborne-lidar-based estimates were also shown to be robust to variations of return density, terrain complexity, and mean canopy height (Figure S10), which supports the applicability of general equations at a regional level, provided that the return density is sufficient to describe the vertical structure and ground surface variability [*Leitold et al.*, 2015]. The results were also consistent among different degradation levels, suggesting that a generalized calibration may be suitable for large areas such as the Brazilian Amazon. We note that airborne lidar data acquisitions were consistent across regions (Table 1), with much higher return densities than many previous studies in tropical forests [e.g., *Asner et al.*, 2012; *Asner and Mascaro*, 2014; *Boyd et al.*, 2013]. Consistent data acquisition, with low variability of flight height and high pulse density, is fundamental to make lidar-derived metrics more robust and comparable across data sets [see also *Næsset*, 2004a, 2004b].

Calibration plots covered a broad geographic range and diversity of degradation histories, contributing to the success of the general airborne-based lidar model (Figure 2). At local scales, however, plots provided an incomplete characterization of carbon stock variability surveyed by the airborne lidar (Figure 5). The airborne lidar survey itself provided detailed information on the variability of forest structure across the landscape. One promising strategy to further improve lidar-based biomass estimates is to acquire the airborne lidar data first then use the data to distribute forest inventory plots across the coverage area to sample a broad range of forest structures with ground-based measurements, thus reducing the risks of excessive extrapolation [*Hawbaker et al.*, 2009; *Maltamo et al.*, 2011; *White et al.*, 2013]. Another promising approach is the use of segmentation techniques to delineate individual trees directly from the point cloud and estimate biomass based on each tree dimensions [*Ferraz et al.*, 2016], possibly accounting for the large variability of biomass explained by crown dimensions [*Goodman et al.*, 2014].

Despite the broad sample of forests in this study, our calibration database and general lidar model under-represent three important forest types. First, study regions in this analysis included few areas with large-scale conventional logging, which is still the most common type of logging in the Amazon [*Sist and Ferreira*, 2007], and thus, our estimates of changes in forest structure, composition, and carbon stocks from logging are likely a lower bound. Second, our study did not include sites in the western and northwestern regions of the Brazilian Amazon. Although these areas are farther away from the arc of deforestation [e.g., *Coe et al.*, 2013], thus less subject to anthropogenic disturbance, these areas also show large uncertainties in biomass and high disagreement in biomass estimates by different regional maps [*Ometto et al.*, 2014]. Third, inventory plots and lidar data in our study targeted *terra firme* Amazon forests; however, at least one sixth of the total Amazon lowland area are wetlands and half of the wetland regions are found in Brazil [*Hess et al.*, 2015]. Efforts to survey carbon stock variability in seasonally flooded forests remain a priority.

4.2. Carbon Debt Associated With Degraded Forests

Degraded and intact forests showed large and persistent differences in carbon density. Even forests affected by low-intensity anthropogenic disturbances such as reduced-impact logging could store significantly less carbon than intact forests. For instance, areas that were logged using reduced-impact techniques stored between 2 and 20% less carbon than intact areas (Figures 5 and 4 and Table 2), and in the case of CAU, differences were still significant 6 years after logging (Figure 5). Without prelogging lidar data, we cannot attribute the observed differences entirely to logging. However, these differences were consistent across all logged areas both at CAU and at other logged sites (Table 2), indicating persistent reductions in ACD from logging [see also *Blanc et al.*, 2009; *West et al.*, 2014; *Rutishauser et al.*, 2015]. Forests subject to conventional logging and especially fires showed more substantial reductions in carbon stocks, and in the most extreme cases of multiple fires more than 90% of the original ACD was lost (Table 2), which further highlights the need to account for the regional impact of forest degradation history on carbon cycle in the Amazon [*Berenguer et al.*, 2014; *Aragão et al.*, 2014; *Bustamante et al.*, 2016].

The persistence of lower aboveground carbon stocks in degraded forests may be linked to long-term effects of disturbance on mortality and on changes in forest structure and composition that prevents short-term recovery. First, fire and logging disturbances also damage trees [e.g., *Veríssimo et al.*, 1992; *Barlow et al.*, 2003], and these are more likely to die in the first years following disturbance [*Barlow et al.*, 2003; *Sist et al.*, 2014]. Also, dead trees contribute to long-term carbon losses due to decomposition [*Keller et al.*, 2004c; *Rice et al.*, 2004; *Palace et al.*, 2007; *Pyle et al.*, 2008; *Anderson et al.*, 2015] and thus further reducing carbon stocks. Second, changes in forest structure and composition following disturbance can alter delay forest

recovery. For example, logging operations disturb and compact soils, which may delay germination [*Karsten et al.*, 2014] and recovery of carbon stocks. Also, both logging and fires increase canopy openings. While canopy openings could accelerate recovery due to increased light penetration, it may also favor the establishment of dense patches of lianas that could halt seedling growth [*Schnitzer et al.*, 2000; *Gerwing and Uhl*, 2002]. Third, changes in forest structure may also make forests more susceptible to subsequent disturbances. Open canopies allow more light to penetrate through canopy, which favors canopy and ground desiccation [*Balch et al.*, 2008]. Drier conditions may increase fire probability and fire intensity, and consequently, mortality rates, especially during years of extreme drought [*Aragão et al.*, 2007; *Brando et al.*, 2014]. Likewise, canopy openness may increase grass invasion, thence forest flammability [*Silvério et al.*, 2013], and increase tree exposure, making them more susceptible to windthrow disturbances [*Silvério*, 2015]. Together, losses through mortality of damaged trees, changes in forest structure and composition, and changes in the forest microenvironment may act to delay or prevent recovery of carbon stocks to predisturbed values at degraded forests.

The magnitude and spatial patterns of carbon stock losses in degraded forests were highly variable, even for forests with similar disturbance histories. Carbon depletion associated with logging ranged from near zero to as much as 49%, and the changes were associated with the intensity and type of logging (Table 2). In addition, the depletion in carbon stocks associated with a single fire event is similar to a recent estimate of about 30% for Amazon forests [*Anderson et al.*, 2015], but our results showed much higher variability (15–53%). While the range of carbon stock depletion due to single logging and single fire events was similar to a ground-based study in the eastern Amazon (18–57%) [*Berenguer et al.*, 2014], when multiple disturbances are included, we found reductions in carbon stocks of more than 90%. One limitation of our study is that we only had one flight per study area obtained after the disturbances had occurred. Therefore, we cannot unequivocally attribute the differences in carbon stocks solely to the previous disturbances or assess recovery after disturbance for older degradation events. However, the large variability in carbon stocks highlights the critical need for an extensive and continuous monitoring of degraded forests to constrain net carbon emissions as a function of logging and burning intensities, recurrence intervals, and interannual variability in the spatial extent of degraded forests [*Morton et al.*, 2013].

4.3. Forest Degradation in Regional Context

The comparison between ALS results and the regional and pantropical maps of aboveground biomass revealed important discrepancies. First, all the three maps tested showed less local heterogeneity than the estimates with lidar (Figure 6), even when lidar estimates were aggregated to 500 m resolution (Figure 7). In the case of *Nogueira et al.* [2015] (N15), the low local variability was expected because the map relies on average values for each landscape, but the lower local variability compared to lidar can also be observed in the *S. S. Saatchi et al.* [2011] (S11) and *Baccini et al.* [2012] (B12). The lower spatial variability of both B12 and S11 maps partially reflects that the data sets used to develop their wall-to-wall maps cannot accurately represent their nominal spatial resolution [*Guitet et al.*, 2015], highlighting the potential for airborne lidar data to provide much needed input for better calibration of regional and global maps of carbon stocks [see also *Baccini and Asner*, 2013; *Marvin et al.*, 2014].

Importantly, the three pan-Amazonian maps consistently showed higher carbon density than the airborne lidar estimates where the top canopy height was low (Figures 6d–6f) and in areas with active disturbance history and low tree cover (Figures 7 and S12). This difference was more pronounced in the case of the N15 map because this map represents potential biomass, but the higher mean and mode for carbon stocks relative to the lidar estimates were also observed with both S11 and B12 maps, particularly in areas affected by fires. One likely explanation for the discrepancy with S11 and B12 maps may be that the correlates used to extrapolate the GLAS-calibrated estimates to the wall-to-wall maps were not sufficiently sensitive to forest degradation. However, differences in the time of reference data are also likely to contribute to the observed bias. The S11 wall-to-wall map was developed using data from 2000 to 2001, and B12 reference data were from 2007 to 2008, whereas the airborne data used in this study were collected between 2012 and 2015. Many of our study areas have been recently affected by fires, logging, and fragmentation since 2001 and 2008 (Table 2), and this consistent difference suggests that recent forest degradation may contribute significantly to carbon stock depletion and carbon emissions in the Amazon from degradation despite declining deforestation rates since 2005. Conversely, for older disturbances that predate the regional maps, airborne lidar predictions of ACD would be higher than regional maps (following forest recovery), which may explain some of the

underestimation by the pantropical maps for older degraded forest classes. Our results indicate the need for frequent updates on the baseline carbon stock maps used in programs such as REDD+ in particular at regions near active land use change.

Spatial variability in Amazon forest carbon stocks impacts REDD+ efforts in three ways. First, degradation processes have distinct and persistent impacts on Amazon forest carbon stocks. Persistent losses may help reporting, because substantial differences exist between degraded and intact forest types over reporting time scales (1–5 years). However, the diversity of spatial patterns in degraded forest carbon stocks will lead to large ranges and high uncertainties without additional mapping, monitoring, and analysis to link degradation type and intensity to forest carbon stocks. For intact forests, spatial variability in forest carbon stocks was not well captured by existing map products—resulting in conservative estimates in the context of REDD+, but underestimates of forest carbon fluxes complicate efforts to characterize Amazon forest carbon dynamics using top-down methods [e.g., *Gatti et al.*, 2014; *van der Laan-Luijkx et al.*, 2015; *Alden et al.*, 2016].

5. Conclusions

Assessing and monitoring carbon stocks in degraded tropical forests is fundamental for successful implementation of REDD+ [*Gibbs et al.*, 2007; *Bustamante et al.*, 2016], and our results show that simple models that integrate ground-based observations and airborne lidar have an excellent potential to characterize variability in tropical forest carbon stocks. Our sampling characterized a variety of forest structure and composition across intact forests and forests subject to different levels of degradation, which allowed us to model and quantify the main differences in carbon stocks associated with intact, logged, and burned forests. Our results also highlight the critical need for developing carbon stock models using remote sensing products that are sensitive to a broad range of forest degradation intensities. The comparison of aboveground biomass carbon estimated from lidar and from previously published pan-Amazonian maps showed important discrepancies and also showed that lidar estimates were consistently lower at areas that have been recently degraded, implying that carbon emissions from forest degradation are an important but highly uncertain component of the Amazon carbon cycle. We provide the first large-scale estimates of carbon losses from forest degradation processes in the Brazilian Amazon. However, variability in carbon stocks within and between degraded forests was based on single surveys at varying time since disturbance. Our results provide important context for degradation losses but do not directly estimate emissions associated with logging and fire. Constraining the uncertainties on degradation-driven carbon emissions in tropical forests is a research priority and will require additional data and continuous monitoring of forest regions that are susceptible to a broad range of logging and fire regimes, including different disturbance intensities and recurrence intervals.

References

Aguiar, A. P. D., et al. (2012), Modeling the spatial and temporal heterogeneity of deforestation-driven carbon emissions: The INPE-EM framework applied to the Brazilian Amazon, *Glob. Change Biol.*, *18*(11), 3346–3366, doi:10.1111/j.1365-2486.2012.02782.x.

Alden, C. B., et al. (2016), Regional atmospheric CO_2 inversion reveals seasonal and geographic differences in Amazon net biome exchange, *Glob. Change Biol.*, *22*, 3427–3443, doi:10.1111/gcb.13305.

Alder, D., J. N. M. Silva, J. O. P. de Carvalho, J. C. Lopes, and A. R. Ruschel (2012), The cohort-empirical modelling strategy and its application to forest management for Tapajós forest, Pará, Brazilian Amazon, *Bois For. Trop.*, *314*(4), 17–23.

Almeida, C. A., A. C. Coutinho, J. C. D. M. Esquerdo, M. Adami, A. Venturieri, C. G. Diniz, N. Dessay, L. Durieux, and A. R. Gomes (2016), High spatial resolution land use and land cover mapping of the Brazilian Legal Amazon in 2008 using Landsat-5/TM and MODIS data, *Acta Amazonica*, *46*(3), 291–302, doi:10.1590/1809-4392201505504.

Andersen, H.-E., S. E. Reutebuch, R. J. McGaughey, M. V. N. d'Oliveira, and M. Keller (2014), Monitoring selective logging in western Amazonia with repeat lidar flights, *Remote Sens. Environ.*, *151*, 157–165, doi:10.1016/j.rse.2013.08.049.

Anderson, L. O., L. E. O. C. Aragão, M. Gloor, E. Arai, M. Adami, S. Saatchi, Y. Malhi, Y. E. Shimabukuro, J. Barlow, E. Berenguer, and V. Duarte (2015), Disentangling the contribution of multiple land covers to fires-mediated carbon emissions in Amazonia during the 2010 drought, *Global Biogeochem. Cycles*, *29*(10), 1739–1753, doi:10.1002/2014GB005008.

Aragão, L. E. O. C., Y. Malhi, R. M. Roman-Cuesta, S. Saatchi, L. O. Anderson, and Y. E. Shimabukuro (2007), Spatial patterns and fire response of recent Amazonian droughts, *Geophys. Res. Lett.*, *34*(7), L07701, doi:10.1029/2006GL028946.

Aragão, L. E. O. C., B. Poulter, J. B. Barlow, L. O. Anderson, Y. Malhi, S. Saatchi, O. L. Phillips, and E. Gloor (2014), Environmental change and the carbon balance of Amazonian forests, *Biol. Rev.*, *89*(4), 913–931, doi:10.1111/brv.12088.

Asner, G. P. (2001), Cloud cover in Landsat observations of the Brazilian Amazon, *Int. J. Remote Sens.*, *22*(18), 3855–3862, doi:10.1080/01431160010006926.

Asner, G. P., and J. Mascaro (2014), Mapping tropical forest carbon: Calibrating plot estimates to a simple LiDAR metric, *Remote Sens. Environ.*, *140*, 614–624, doi:10.1016/j.rse.2013.09.023.

Asner, G. P., M. Keller, R. Pereira, J. C. Zweede Jr., and J. N. M. Silva (2004), Canopy damage and recovery after selective logging in Amazonia: Field and satellite studies, *Ecol. Appl.*, *14*(SP4), 280–298, doi:10.1890/01-6019.

Asner, G. P., D. E. Knapp, E. N. Broadbent, P. J. C. Oliveira, M. Keller, and J. N. Silva (2005), Selective logging in the Brazilian Amazon, *Science*, *310*(5747), 480–482, doi:10.1126/science.1118051.

Asner, G. P., et al. (2010), High-resolution forest carbon stocks and emissions in the Amazon, *Proc. Natl. Acad. Sci. U.S.A.*, *107*(38), 16,738–16,742, doi:10.1073/pnas.1004875107.

Asner, G. P., J. Mascaro, H. C. Muller-Landau, G. Vieilledent, R. Vaudry, M. Rasamoelina, J. S. Hall, and M. Breugel (2012), A universal airborne LiDAR approach for tropical forest carbon mapping, *Oecologia*, *168*(4), 1147–1160, doi:10.1007/s00442-011-2165-z.

Baccini, A., and G. P. Asner (2013), Improving pantropical forest carbon maps with airborne LiDAR sampling, *Carbon Manage.*, *4*(6), 591–600, doi:10.4155/cmt.13.66.

Baccini, A., et al. (2012), Estimated carbon dioxide emissions from tropical deforestation improved by carbon-density maps, *Nat. Clim. Change*, *2*(3), 182–185, doi:10.1038/nclimate1354.

Balch, J. K., D. C. Nepstad, P. M. Brando, L. M. Curran, O. Portela, O. de Carvalho, and P. Lefebvre (2008), Negative fire feedback in a transitional forest of southeastern Amazonia, *Glob. Change Biol.*, *14*(10), 2276–2287, doi:10.1111/j.1365-2486.2008.01655.x.

Barber, C. P., M. A. Cochrane, C. M. Souza Jr., and W. F. Laurance (2014), Roads, deforestation, and the mitigating effect of protected areas in the Amazon, *Biol. Conserv.*, *177*, 203–209, doi:10.1016/j.biocon.2014.07.004.

Barlow, J., C. A. Peres, B. O. Lagan, and T. Haugaasen (2003), Large tree mortality and the decline of forest biomass following Amazonian wildfires, *Ecol. Lett.*, *6*(1), 6–8, doi:10.1046/j.1461-0248.2003.00394.x.

Batistella, M., E. L. Bolfe, and E. F. Moran (2013), Agroforestry in Tomé-Açu: An alternative to pasture in the Amazon, in *Human-Environment Interactions: Current and Future Directions*, edited by E. S. Brondízio and E. F. Moran, pp. 321–342, chap 14, Springer Netherlands, Dordrecht, Netherlands, doi:10.1007/978-94-007-4780-7.

Berenguer, E., J. Ferreira, T. A. Gardner, L. E. O. C. Aragão, P. B. de Camargo, C. E. Cerri, M. Durigan, R. C. D. Oliveira, I. C. G. A. Vieira, and J. Barlow (2014), A large-scale field assessment of carbon stocks in human-modified tropical forests, *Glob. Change Biol.*, *20*(12), 3713–3726, doi:10.1111/gcb.12627.

Blanc, L., M. Echard, B. Hérault, D. Bonal, E. Marcon, J. Chave, and C. Baraloto (2009), Dynamics of aboveground carbon stocks in a selectively logged tropical forest, *Ecol. Appl.*, *19*(6), 1397–1404, doi:10.1890/08-1572.1.

Boyd, D. S., R. A. Hill, C. Hopkinson, and T. R. Baker (2013), Landscape-scale forest disturbance regimes in southern Peruvian Amazonia, *Ecol. Appl.*, *23*(7), 1588–1602, doi:10.1890/12-0371.1.

Brando, P. M., et al. (2014), Abrupt increases in Amazonian tree mortality due to drought–fire interactions, *Proc. Natl. Acad. Sci. U.S.A.*, *111*(17), 6347–6352, doi:10.1073/pnas.1305499111.

Breiman, L. (2001), Random forests, *Mach. Learn.*, *45*(1), 5–32, doi:10.1023/A:1010933404324.

Bustamante, M. M. C., et al. (2016), Towards an integrated monitoring framework to assess the effects of tropical forest degradation and recovery on carbon stocks and biodiversity, *Glob. Change Biol.*, *22*(1), 92–109, doi:10.1111/gcb.13087.

Chambers, J. Q., N. Higuchi, J. P. Schimel, L. V. Ferreira, and J. M. Melack (2000), Decomposition and carbon cycling of dead trees in tropical forests of the central Amazon, *Oecologia*, *122*(3), 380–388, doi:10.1007/s004420050044.

Chauvel, A., Y. Lucas, and R. Boulet (1987), On the genesis of the soil mantle of the region of Manaus, Central Amazonia, Brazil, *Experientia*, *43*(3), 234–241, doi:10.1007/BF01945546.

Chave, J., R. Condit, S. Aguilar, A. Hernandez, S. Lao, and R. Perez (2004), Error propagation and scaling for tropical forest biomass estimates, *Philos. Trans. R. Soc. London, Ser. B*, *359*(1443), 409–420, doi:10.1098/rstb.2003.1425.

Chave, J., D. Coomes, S. Jansen, S. L. Lewis, N. G. Swenson, and A. E. Zanne (2009), Towards a worldwide wood economics spectrum, *Ecol. Lett.*, *12*(4), 351–366, doi:10.1111/j.1461-0248.2009.01285.x.

Chave, J., et al. (2014), Improved allometric models to estimate the aboveground biomass of tropical trees, *Glob. Change Biol.*, *20*(10), 3177–3190, doi:10.1111/gcb.12629.

Coe, M. T., et al. (2013), Deforestation and climate feedbacks threaten the ecological integrity of South–Southeastern Amazonia, *Philos. Trans. R Soc. Lond. B Biol. Sci.*, *368*(1619), 20120155, doi:10.1098/rstb.2012.0155.

de Castilho, C. V., W. E. Magnusson, R. N. O. de Araújo, R. C. C. Luizão, F. J. Luizão, A. P. Lima, and N. Higuchi (2006), Variation in aboveground tree live biomass in a central Amazonian forest: Effects of soil and topography, *Forest Ecol. Manage.*, *234*(1–3), 85–96, doi:10.1016/j.foreco.2006.06.024.

De'ath, G. (2007), Boosted trees for ecological modeling and prediction, *Ecology*, *88*(1), 243–251, doi:10.1890/0012-9658(2007)88[243:BTFEMA]2.0.CO;2.

d'Oliveira, M. V. N., S. E. Reutebuch, R. J. McGaughey, and H.-E. Andersen (2012), Estimating forest biomass and identifying low-intensity logging areas using airborne scanning lidar in Antimary State Forest, Acre state, western Brazilian Amazon, *Remote Sens. Environ.*, *124*, 479–491, doi:10.1016/j.rse.2012.05.014.

dos-Santos, M. N., and M. Keller (2016a), *CMS: Forest Inventory and Biophysical Measurements, Pará, Brazil, 2012–2014*, Oak Ridge National Laboratory Distributed Active Archive Center, Oak Ridge, Tenn.

dos-Santos, M. N., and M. Keller (2016b), *CMS: LiDAR Data for Forested Areas in Paragominas, Pará, Brazil, 2012–2014*, Oak Ridge National Laboratory Distributed Active Archive Center, Oak Ridge, Tenn.

EBATA (2012), Plano operacional anual—UMF II, Floresta Nacional Saracá-Taquera, Oriximiná, Pará, Activities Rep., Ebata Produtos Florestais Ltda., Belém, PA, Brazil.

Efron, B., and R. Tibshirani (1997), Improvements on cross-validation: The 632+ bootstrap method, *J. Am. Stat. Assoc.*, *92*(438), 548–560, doi:10.2307/2965703.

Feldpausch, T. R., et al. (2012), Tree height integrated into pantropical forest biomass estimates, *Biogeosciences*, *9*(8), 3381–3403, doi:10.5194/bg-9-3381-2012.

Ferraz, A., S. Saatchi, C. Mallet, and V. Meyer (2016), Lidar detection of individual tree size in tropical forests, *Remote Sens. Environ.*, *183*, 318–333, doi:10.1016/j.rse.2016.05.028.

Gatti, L. V., et al. (2014), Drought sensitivity of Amazonian carbon balance revealed by atmospheric measurements, *Nature*, *506*(7486), 76–80, doi:10.1038/nature12957.

Gerwing, J. J., and C. Uhl (2002), Pre-logging liana cutting reduces liana regeneration in logging gaps in the Eastern Brazilian Amazon, *Ecol. Appl.*, *12*(6), 1642–1651, doi:10.1890/1051-0761(2002)012[1642:PLLCRL]2.0.CO;2.

Gibbs, H. K., B. Sandra, J. O. Niles, and J. A. Foley (2007), Monitoring and estimating tropical forest carbon stocks: Making REDD a reality, *Environ. Res. Lett.*, *2*(4), 045023, doi:10.1088/1748-9326/2/4/045023.

Goodman, R. C., O. L. Phillips, D. C. Torres, L. Freitas, S. T. Cortese, A. Monteagudo, and T. R. Baker (2013), Amazon palm biomass and allometry, *Forest Ecol. Manag.*, *310*, 994–1004, doi:10.1016/j.foreco.2013.09.045.

Goodman, R. C., O. L. Phillips, and T. R. Baker (2014), The importance of crown dimensions to improve tropical tree biomass estimates, *Ecol. Appl.*, *24*(4), 680–698, doi:10.1890/13-0070.1.

Guimarães, J., A. Veríssimo, P. Amaral, and A. Demachki (2011), *Municípios Verdes: Caminhos Para a Sustentabilidade*, Instituto do Homem e Meio Ambiente da Amazônia – Imazon, Belém, PA, Brazil.

Guitet, S., B. Hérault, Q. Molto, O. Brunaux, and P. Couteron (2015), Spatial structure of above-ground biomass limits accuracy of carbon mapping in rainforest but large scale forest inventories can help to overcome, *PLoS One*, *10*(9), E0138456, doi:10.1371/journal.pone.0138456.

Hansen, M. C., J. R. G. Townshend, R. S. DeFries, and M. Carroll (2005), Estimation of tree cover using MODIS data at global, continental and regional/local scales, *Int. J. Remote Sens.*, *26*(19), 4359–4380, doi:10.1080/01431160500113435.

Hansen, M. C., et al. (2013), High-resolution global maps of 21st-century forest cover change, *Science*, *342*(6160), 850–853, doi:10.1126/science.1244693.

Harmon, M. E., D. F. Whigham, J. Sexton, and I. Olmsted (1995), Decomposition and mass of woody detritus in the dry tropical forests of the Northeastern Yucatan Peninsula, Mexico, *Biotropica*, *27*(3), 305–316, doi:10.2307/2388916.

Hawbaker, T. J., N. S. Keuler, A. A. Lesak, T. Gobakken, K. Contrucci, and V. C. Radeloff (2009), Improved estimates of forest vegetation structure and biomass with a LiDAR-optimized sampling design, *J. Geophys. Res.*, *114*, G00E04, doi:10.1029/2008JG000870.

Hess, L. L., J. M. Melack, A. G. Affonso, C. Barbosa, M. Gastil-Buhl, and E. M. L. M. Novo (2015), Wetlands of the lowland Amazon Basin: Extent, vegetative cover, and dual-season inundated area as mapped with JERS-1 synthetic aperture radar, *Wetlands*, *35*(4), 745–756, doi:10.1007/s13157-015-0666-y.

Hudak, A. T., N. L. Crookston, J. S. Evans, M. J. Falkowski, A. M. S. Smith, P. E. Gessler, and P. Morgan (2006), Regression modeling and mapping of coniferous forest basal area and tree density from discrete-return lidar and multispectral satellite data, *Can. J. Remote Sens.*, *32*(2), 126–138, doi:10.5589/m06-007.

Hudak, A. T., E. K. Strand, L. A. Vierling, J. C. Byrne, J. U. Eitel, S. Martinuzzi, and M. J. Falkowski (2012), Quantifying aboveground forest carbon pools and fluxes from repeat LiDAR surveys, *Remote Sens. Environ.*, *123*, 25–40, doi:10.1016/j.rse.2012.02.023.

Hunter, M. O., M. Keller, D. Vitoria, and D. C. Morton (2013), Tree height and tropical forest biomass estimation, *Biogeosciences*, *10*(6), 10,491–10,529, doi:10.5194/bg-10-8385-2013.

IBAMA (2004), Floresta Nacional do Tapajós: Plano de manejo, Government Rep., Brazilian Ministry of Envrioment.

IBGE (2012), Manual técnico da vegetação brasileira. 2ª edição, Tech. Rep., Fundação Instituto Brasileiro de Geografia e Estatística, Rio de Janeiro, Brazil.

INPE (2014), Mapeamento da degradação florestal na Amazônia brasileira (DEGRAD). [Available at http://www.obt.inpe.br/degrad/.]

Jakubowski, M. K., Q. Guo, and M. Kelly (2013), Tradeoffs between lidar pulse density and forest measurement accuracy, *Remote Sens. Environ.*, *130*, 245–253, doi:10.1016/j.rse.2012.11.024.

Joshi, N., E. T. A. Mitchard, N. Woo, J. Torres, J. Moll-Rocek, A. Ehammer, M. Collins, M. R. Jepsen, and R. Fensholt (2015), Mapping dynamics of deforestation and forest degradation in tropical forests using radar satellite data, *Environ. Res. Lett.*, *10*(3), 034014, doi:10.1088/1748-9326/10/3/034014.

Karsten, R. J., H. Meilby, and J. B. Larsen (2014), Regeneration and management of lesser known timber species in the Peruvian Amazon following disturbance by logging, *Forest Ecol. Manage.*, *327*, 76–85, doi:10.1016/j.foreco.2014.04.035.

Keller, M., G. P. Asner, N. Silva, and M. Palace (2004a), Sustainability of selective logging of upland forest in the Brazilian Amazon, in *Working forests in the Neotropics: Conservation through sustainable management?*, edited by D. J. Zarin et al., pp. 41–63, chap 4., Columbia Univ. Press, New York.

Keller, M., et al. (2004b), Ecological research in the large-scale biosphere–atmosphere experiment in Amazonia: Early results, *Ecol. Appl.*, *14*(SP4), 3–16, doi:10.1890/03-6003.

Keller, M., M. Palace, G. P. Asner, R. Pereira, and J. N. M. Silva (2004c), Coarse woody debris in undisturbed and logged forests in the Eastern Brazilian Amazon, *Glob. Change Biol.*, *10*(5), 784–795, doi:10.1111/j.1529-8817.2003.00770.x.

Langner, A., F. Achard, and G. Grassi (2014), Can recent pan-tropical biomass maps be used to derive alternative Tier 1 values for reporting REDD+ activities under UNFCCC?, *Environ. Res. Lett.*, *9*(12), 124008, doi:10.1088/1748-9326/9/12/124008.

Lapola, D. M., et al. (2014), Pervasive transition of the Brazilian land-use system, *Nat. Clim. Change*, *4*(1), 27–35, doi:10.1038/nclimate2056.

Le Quéré, C., et al. (2015), Global carbon budget, *Earth Syst. Sci. Data*, *7*(2), 349–396, doi:10.5194/essd-7-349-2015.

Leitold, V., M. Keller, D. Morton, B. Cook, and Y. Shimabukuro (2015), Airborne lidar-based estimates of tropical forest structure in complex terrain: Opportunities and trade-offs for REDD+, *Carbon Balance Manage.*, *10*(3), 1–12, doi:10.1186/s13021-015-0013-x.

Lewis, S. L., P. M. Brando, O. L. Phillips, G. M. F. van der Heijden, and D. Nepstad (2011), The 2010 Amazon drought, *Science*, *331*(6017), 554, doi:10.1126/science.1200807.

Liaw, A., and M. Wiener (2002), Classification and regression by random forest, *R News*, *2*(3), 18–22.

Liu, Z., D. Ostrenga, W. Teng, and S. Kempler (2012), Tropical Rainfall Measuring Mission (TRMM) precipitation data and services for research and applications, *Bull. Am. Meteorol. Soc.*, *93*(9), 1317–1325, doi:10.1175/BAMS-D-11-00152.1.

Lloyd, A. H., P. A. Duffy, and D. H. Mann (2013), Nonlinear responses of white spruce growth to climate variability in interior Alaska, *Can. J. Forest Res.*, *43*(4), 331–343, doi:10.1139/cjfr-2012-0372.

MADEFLONA (2010), Plano operacional anual 2010—UMF I. Floresta Nacional Jamari, Itapuã d'Oeste, Rondônia, *Activities Rep.*, MADEFLONA Industrial Madeireira Ltda., Itapuã d'Oeste, RO, Brazil.

Maltamo, M., O. M. Bollandsås, E. Næsset, T. Gobakken, and P. Packalén (2011), Different plot selection strategies for field training data in ALS-assisted forest inventory, *Forestry*, *84*(1), 23–31, doi:10.1093/forestry/cpq039.

Marvin, D. C., G. P. Asner, D. E. Knapp, C. B. Anderson, R. E. Martin, F. Sinca, and R. Tupayachi (2014), Amazonian landscapes and the bias in field studies of forest structure and biomass, *Proc. Natl. Acad. Sci. U.S.A.*, *111*(48), E5224—E5232, doi:10.1073/pnas.1412999111.

Mascaro, J., C. M. Litton, R. F. Hughes, A. Uowolo, and S. A. Schnitzer (2011a), Minimizing bias in biomass allometry: Model selection and log-transformation of data, *Biotropica*, *43*(6), 649–653, doi:10.1111/j.1744-7429.2011.00798.x.

Mascaro, J., M. Detto, G. P. Asner, and H. C. Muller-Landau (2011b), Evaluating uncertainty in mapping forest carbon with airborne LiDAR, *Remote Sens. Environ.*, *115*(12), 3770–3774, doi:10.1016/j.rse.2011.07.019.

Mascaro, J., G. P. Asner, D. E. Knapp, T. Kennedy-Bowdoin, R. E. Martin, C. Anderson, M. Higgins, and K. D. Chadwick (2014), A tale of two "forests": Random forest machine learning aids tropical forest carbon mapping, *PLoS One*, *9*(1), E85993, doi:10.1371/journal.pone.0085993.

Mason, D. M., and J. H. Schuenemeyer (1983), A modified Kolmogorov-Smirnov test sensitive to tail alternatives, *Ann. Stat.*, *11*(3), 933–946, doi:10.1214/aos/1176346259.

Mauya, E., E. Hansen, T. Gobakken, O. Bollandsas, R. Malimbwi, and E. Næsset (2015), Effects of field plot size on prediction accuracy of aboveground biomass in airborne laser scanning-assisted inventories in tropical rain forests of Tanzania, *Carbon Balance Manage.*, *10*(10), 1–14, doi:10.1186/s13021-015-0021-x.

McGaughey, R. J. (2014), *FUSION/LDV: Software for LIDAR Data Analysis and Visualization*, Manual, USFS Pacific Northwest Research Station, Seattle, Wash.

Meyer, V., S. S. Saatchi, J. Chave, J. W. Dalling, S. Bohlman, G. A. Fricker, C. Robinson, M. Neumann, and S. Hubbell (2013), Detecting tropical forest biomass dynamics from repeated airborne lidar measurements, *Biogeosciences*, *10*(8), 5421–5438, doi:10.5194/bg-10-5421-2013.

Miller, A. J. (1984), Selection of subsets of regression variables, *J. R. Stat. Soc.*, *147*(3), 389–425, doi:10.2307/2981576.

Molina, P. X., G. P. Asner, M. Farjas Abadía, J. C. Ojeda Manrique, L. A. Sánchez Diez, and R. Valencia (2016), Spatially-explicit testing of a general aboveground carbon density estimation model in a Western Amazonian forest using airborne LiDAR, *Remote Sens.*, *8*(1), 9, doi:10.3390/rs8010009.

Morton, D. C. (2016), Forest carbon fluxes: A satellite perspective, *Nat. Clim. Change*, *6*(4), 346–348, doi:10.1038/nclimate2978.

Morton, D. C., Y. Le Page, R. S. DeFries, G. J. Collatz, and G. C. Hurtt (2013), Understorey fire frequency and the fate of burned forests in southern Amazonia, *Phil. Trans. R. Soc. B*, *368*, 20120163, doi:10.1098/rstb.2012.0163.

Næsset, E. (2004a), Accuracy of forest inventory using airborne laser scanning: Evaluating the first nordic full-scale operational project, *Scand. J. For. Res.*, *19*(6), 554–557, doi:10.1080/02827580410019544.

Næsset, E. (2004b), Effects of different flying altitudes on biophysical stand properties estimated from canopy height and density measured with a small-footprint airborne scanning laser, *Remote Sens. Environ.*, *91*(2), 243–255, doi:10.1016/j.rse.2004.03.009.

Nepstad, D., et al. (2014), Slowing Amazon deforestation through public policy and interventions in beef and soy supply chains, *Science*, *344*(6188), 1118–1123, doi:10.1126/science.1248525.

Nogueira, E. M., P. M. Fearnside, B. W. Nelson, R. I. Barbosa, and E. W. H. Keizer (2008), Estimates of forest biomass in the Brazilian Amazon: New allometric equations and adjustments to biomass from wood-volume inventories, *Forest Ecol. Manag.*, *256*(11), 1853–1867, doi:10.1016/j.foreco.2008.07.022.

Nogueira, E. M., A. M. Yanai, F. O. R. Fonseca, and P. M. Fearnside (2015), Carbon stock loss from deforestation through 2013 in Brazilian Amazonia, *Glob. Change Biol.*, *21*(3), 1271–1292, doi:10.1111/gcb.12798.

Ometto, J. P., A. P. Aguiar, T. Assis, L. Soler, P. Valle, G. Tejada, D. M. Lapola, and P. Meir (2014), Amazon forest biomass density maps: Tackling the uncertainty in carbon emission estimates, *Clim. Change*, *124*(3), 545–560, doi:10.1007/s10584-014-1058-7.

Palace, M., M. Keller, G. P. Asner, J. N. M. Silva, and C. Passos (2007), Necromass in undisturbed and logged forests in the Brazilian Amazon, *Forest Ecol. Manage.*, *238*(1–3), 309–318, doi:10.1016/j.foreco.2006.10.026.

Phillips, S. J., R. P. Anderson, and R. E. Schapire (2006), Maximum entropy modeling of species geographic distributions, *Ecol. Model.*, *190*(3–4), 231–259, doi:10.1016/j.ecolmodel.2005.03.026.

Pinto, A., P. Amaral, C. M. Souza Jr., A. Veríssimo, R. Salomão, G. Gomes, and C. Balieiro (2009), Diagnóstico socioeconômico e florestal do município de Paragominas, Tech. Rep., Instituto do Homem e Meio Ambiente da Amazônia (Imazon), Belém, PA, Brazil.

Pütz, S., J. Groeneveld, K. Henle, C. Knogge, A. C. Martensen, M. Metz, J. P. Metzger, M. C. Ribeiro, M. D. de Paula, and A. Huth (2014), Long-term carbon loss in fragmented Neotropical forests, *Nat. Commun.*, *5*, 5037, doi:10.1038/ncomms6037.

Pyle, E. H., et al. (2008), Dynamics of carbon, biomass, and structure in two Amazonian forests, *J. Geophys. Res.*, *113*(G1), G00B08, doi:10.1029/2007JG000592.

R Core Team (2015), *R: A Language and Environment for Statistical Computing*, R Foundation for Statistical Computing, Vienna, Austria.

Réjou-Méchain, M., B. Tymen, L. Blanc, S. Fauset, T. R. Feldpausch, A. Monteagudo, O. L. Phillips, H. Richard, and J. Chave (2015), Using repeated small-footprint LiDAR acquisitions to infer spatial and temporal variations of a high-biomass Neotropical forest, *Remote Sens. Environ.*, *169*, 93–101, doi:10.1016/j.rse.2015.08.001.

Rice, A., E. Pyle, S. Saleska, L. Hutyra, M. Palace, M. Keller, P. de Camargo, K. Portilho, D. Marques, and S. Wofsy (2004), Carbon balance and vegetation dynamics in an old-growth Amazonian forest, *Ecol. Appl.*, *14*(S4), S55—S71, doi:10.1890/02-6006.

Ridgeway, G. (2015), *GBM: Generalized Boosted Regression Models*, R package version 2.1.1. With contributions from others. [Available at https://github.com/gbm-developers/gbm.]

Rutishauser, E., et al. (2015), Rapid tree carbon stock recovery in managed Amazonian forests, *Curr. Biol.*, *25*(18), R787—R788, doi:10.1016/j.cub.2015.07.034.

Rutishauser, E., B. Hérault, P. Petronelli, and P. Sist (2016), Tree height reduction after selective logging in a tropical forest, *Biotropica*, *48*(3), 285–289, doi:10.1111/btp.12326.

Saatchi, S., M. Marlier, R. L. Chazdon, D. B. Clark, and A. E. Russell (2011), Impact of spatial variability of tropical forest structure on radar estimation of aboveground biomass, *Remote Sens. Environ.*, *115*(11), 2836–2849, doi:10.1016/j.rse.2010.07.015.

Saatchi, S. S., R. A. Houghton, R. C. D. S. Alvalá, J. V. Soares, and Y. Yu (2007), Distribution of aboveground live biomass in the Amazon basin, *Glob. Change Biol.*, *13*(4), 816–837, doi:10.1111/j.1365-2486.2007.01323.x.

Saatchi, S. S., et al. (2011), Benchmark map of forest carbon stocks in tropical regions across three continents, *Proc. Natl. Acad. Sci. U.S.A.*, *108*(24), 9899–9904, doi:10.1073/pnas.1019576108.

Sabine, C. L., et al. (2004), Current status and past trends of the global carbon cycle, in *The Global Carbon Cycle: Integrating Humans, Climate, and the Natural World, Scientific Committee on Problems of the Environment*, vol. 62, edited by C. B. Field and M. R. Raupach, pp. 17–44, chap. 2, Island Press, Washington, D. C.

Schnitzer, S. A., J. W. Dalling, and W. P. Carson (2000), The impact of lianas on tree regeneration in tropical forest canopy gaps: Evidence for an alternative pathway of gap-phase regeneration, *J. Ecol.*, *88*(4), 655–666, doi:10.1046/j.1365-2745.2000.00489.x.

Schnitzer, S. A., S. J. DeWalt, and J. Chave (2006), Censusing and measuring lianas: A quantitative comparison of the common methods, *Biotropica*, *38*(5), 581–591, doi:10.1111/j.1744-7429.2006.00187.x.

Schwarz, G. (1978), Estimating the dimension of a model, *Ann. Stat.*, *6*(2), 461–464, doi:10.1214/aos/1176344136.

Silvério, D. (2015), Alterações na estrutura e funcionamento de florestas transicionais na Amazônia associadas à degradação florestal e transições no uso da terra, PhD thesis, Univ. of Brasília, Brasília, Brazil.

Silvério, D. V., P. M. Brando, J. K. Balch, F. E. Putz, D. C. Nepstad, C. Oliveira-Santos, and M. M. C. Bustamante (2013), Testing the Amazon savannization hypothesis: Fire effects on invasion of a neotropical forest by native cerrado and exotic pasture grasses, *Philos. Trans. R. Soc. B*, *368*, 20120427, doi:10.1098/rstb.2012.0427.

Sist, P., and F. N. Ferreira (2007), Sustainability of reduced-impact logging in the Eastern Amazon, *Forest Ecol. Manage.*, *243*(2–3), 199–209, doi:10.1016/j.foreco.2007.02.014.

Sist, P., L. Mazzei, L. Blanc, and E. Rutishauser (2014), Large trees as key elements of carbon storage and dynamics after selective logging in the Eastern Amazon, *Forest Ecol. Manage.*, *318*, 103–109, doi:10.1016/j.foreco.2014.01.005.

Slik, J. W. F., et al. (2013), Large trees drive forest aboveground biomass variation in moist lowland forests across the tropics, *Global Ecol. Biogeogr.*, *22*(12), 1261–1271, doi:10.1111/geb.12092.

Smith, P., et al. (2014), Agriculture, forestry and other land use (AFOLU), in *Climate Change 2014: Mitigation of Climate Change. Contribution of Working Group III to the Fifth Assessment Report of the Intergovernmental Panel on Climate Change*, vol. 11, edited by O. Edenhofer et al., pp. 811–922, Cambridge Univ. Press, Cambridge U. K. and New York.

Townshend, J. R. G., M. Carroll, C. Dimiceli, R. Sohlberg, M. C. Hansen, and R. S. DeFries (2001), Vegetation Continuous Fields MOD44B, 2012 and 2013 percent tree cover, Collection 5. [Available at http://reverb.echo.nasa.gov.]

UN-FCCC (2016), Report of the conference of the parties on its twenty-first session, held in Paris from 30 November to 13 December 2015. Part two: Action taken by the conference of the parties at its twenty-first session, Report FCCC/CP/2015/10/Add.1, United Nations Framework Convention on Climate Change, Paris.

van der Laan-Luijkx, I. T., et al. (2015), Response of the Amazon carbon balance to the 2010 drought derived with CarbonTracker South America, *Global Biogeochem. Cycles*, *29*(7), 1092–1108, doi:10.1002/2014GB005082.

van der Werf, G. R., D. C. Morton, R. S. DeFries, J. G. J. Olivier, P. S. Kasibhatla, R. B. Jackson, G. J. Collatz, and J. T. Randerson (2009), CO_2 emissions from forest loss, *Nature Geosci.*, *2*(11), 737–738, doi:10.1038/ngeo671.

Veríssimo, A., P. Barreto, M. Mattos, R. Tarifa, and C. Uhl (1992), Logging impacts and prospects for sustainable forest management in an old Amazonian frontier: The case of Paragominas, *Forest Ecol. Manage.*, *55*(1–4), 169–199, doi:10.1016/0378-1127(92)90099-U.

Vincent, G., D. Sabatier, and E. Rutishauser (2014), Revisiting a universal airborne light detection and ranging approach for tropical forest carbon mapping: Scaling-up from tree to stand to landscape, *Oecologia*, *175*(2), 439–443, doi:10.1007/s00442-014-2913-y.

West, T. A. P., E. Vidal, and F. E. Putz (2014), Forest biomass recovery after conventional and reduced-impact logging in Amazonian Brazil, *Forest Ecol. Manage.*, *314*, 59–63, doi:10.1016/j.foreco.2013.11.022.

White, J. C., M. A. Wulder, A. Varhola, M. Vastaranta, N. C. Coops, B. D. Cook, D. Pitt, and M. Woods (2013), A best practices guide for generating forest inventory attributes from airborne laser scanning data using an area-based approach (version 2.0), *Information Rep.*, Canadian Wood Fibre Centre, Victoria, British Columbia, Canada.

Zanne, A. E., G. Lopez-Gonzalez, D. A. Coomes, J. Ilic, S. Jansen, S. L. Lewis, R. B. Miller, N. G. Swenson, M. C. Wiemann, and J. Chave (2009), Data from: Towards a worldwide wood economics spectrum, *Dryad Data Repository*, doi:10.5061/dryad.234.